Université de Montréal

Classification de pollens par réseau neuronal :

Application en reconstructions paléo-environnementales de populations marginales

Par

Médéric Durand

Département de géographie, Faculté des Arts et Sciences

Mémoire présenté en vue de l'obtention du grade de Maîtrise ès sciences en Géographie environnementale

Avril 2023

Université de Montréal
Département de géographie, Faculté des Arts et Sciences

Ce mémoire intitulé

Classification de pollens par réseau neuronal :
Application en reconstructions paléo-environnementales de populations marginales

Présenté par
Médéric Durand

A été évalué par un jury composé des personnes suivantes

Julie Talbot
Présidente-rapporteuse

Olivier Blarquez
Directeur de recherche

Pierre Grondin
Codirecteur

Matthew Peros
Membre du jury

RÉSUMÉ

La hausse actuelle du climat pousse les espèces d'arbres tempérés à migrer vers le nord. En vue de comprendre comment certaines espèces réagiront face à cette migration, nous pouvons porter notre regard vers les populations marginales. Les études paléoécologiques de ces populations – situées au-delà de l'aire de répartition continue de l'espèce – peuvent nous informer quant aux conditions écologiques nécessaires à leur migration. Ce mémoire analyse un peuplement d'érables à sucre (*Acer saccharum* Marsh.) situé à la limite nordique de la répartition de l'espèce, dans la forêt tempérée mixte québécoise. L'objectif de la recherche est d'identifier quand et sous quelles conditions écologiques *A. saccharum* s'est établi en situation marginale.

À ces fins, cette étude propose l'analyse des fossiles extraits des sédiments lacustres d'un lac situé à proximité de l'érablière. Un modèle d'apprentissage-machine est entraîné à l'aide d'images de pollens et permet la classification des pollens extraits des sédiments lacustres – le premier de la sorte. Notre méthode proposée emploi un protocole d'extraction fossile accéléré et des réseaux de neurone convolutifs permettant de classifier les pollens des espèces les plus retrouvées dans les sédiments quaternaires du nord-est de l'Amérique. Bien qu'encore incapable de classifier précisément toutes les espèces présentes dans une telle séquence fossile, notre modèle est une preuve de concept envers l'automatisation de la paléo-palynologie.

Les résultats produits par le modèle combinés à l'analyse des charbons fossiles permettent la reconstruction de la végétation et des feux des 10,000 dernières années. L'établissement régional d'*A. saccharum* est daté à 4,800 cal. BP, durant une période de refroidissement climatique et de feux fréquents mais de faible sévérité. Sa présence locale est prudemment établie à 1,200 cal. BP. Les résultats de ce mémoire soulignent le potentiel de la paléo-palynologie automatique ainsi que la complexité de l'écologie d'*A. saccharum*.

Mots-clés : Paléoécologie, *Acer saccharum*, palynologie automatique, Réseaux de neurone convolutifs (CNN), histoire des feux, Québec

ABSTRACT

The current global climate warming is pushing temperate tree species to migrate northwards. To understand how certain species will undergo this migration, we can look at marginal populations. The paleoecological studies of such populations, located beyond the species' core distribution range, can inform us of the conditions needed for a successful migration. This research thesis analyses a sugar maple (*Acer saccharum* Marsh.) stand located at the northern boundary of the species' limit, in Québec's mixed-temperate forest. The objective of this research is to identify when and under which ecological conditions did *A. saccharum* establish itself as the stand's dominant species.

To that end, this study analyses the fossil record found in a neighbouring lake's organic sediments. A machine learning-powered model is trained using pollen images to classify the lacustrine sediment's pollen record. The first of its kind, our proposed method employs an accelerated fossil pollen extraction protocol and convolutional neural networks and can classify the species most commonly found in Northeastern American Quaternary fossil records. Although not yet capable of accurately classifying a complete fossil pollen sequence, our model serves as a proof of concept towards automation in paleo-palynology.

Using results generated by our model combined with the analysis of the fossil charcoal record, the past 10,000 years of vegetation and fire history is reconstructed. The regional establishment of *A. saccharum* is conservatively dated at 4,800 cal. BP, during a period of climate cooling and frequent, although non-severe, forest fires. Its local presence can only be attested to since 1,200 cal. BP. This thesis' results highlight both the potential of automated paleo-palynology and the complexity of *A. saccharum*'s ecological requirements.

Keywords: Paleoecology, *Acer saccharum*, Automated palynology, Convolutional Neural Networks, Fire history, Québec

TABLE DES MATIÈRES

TABLE DES FIGURES

LISTE DES TABLEAUX

SIGLES ET ABRÉVIATIONS

α : Risque d'erreur/niveau de signification

μ : Mu / moyenne d'une population

μm : Micromètre

μl : Microlitre

14-C : Isotope du carbone utilisé pour la datation (Carbone 14 / C^{14})

APC : Précision moyenne par classe (*Average per-class accuracy*)

Cal. BP : Années calibrées avant le présent (*Before Present;* avant 1950)

CE : Ère commune (*Common Era*; après l'an -1)

Char Acc : Accumulation de charbon fossiles dans les sédiments (mm^{-2} . cm^{-2} . $année^{-1}$)

CNN : Réseau de neurone convolutif (*Convolutional Neural Network*)

CONISS : Analyse de zonation stratigraphique

NLL : *Negative log likelihood*

NPP : Non-pollen palynomorph

OCH : Optimum climatique Holocène

R^2 : R-carré / Coefficient de détermination

RMSE : Racine de l'erreur quadratique moyenne (*Root-mean-square deviation*)

RPM : Rotation par minute (*Rotation per minute*)

T : Température (indice scalaire permettant la calibration)

REMERCIEMENTS

Un grand merci à Pierre Grondin, qui a su m'encadrer à coup d'attitude positive, de détermination et d'une connaissance encyclopédique du fonctionnement de nos forêts. Je dis merci à mon directeur Olivier Blarquez, qui m'a offert une introduction sans pareil au monde de la recherche en environnement.

Je remercie aussi les collègues du feu laboratoire de paléoécologie – Julie A. et Andy pour leur bienveillance durant mes débuts au labo, et tout particulièrement Jordan, qui se mérite le titre honorifique de co-co-directeur – Sans oublier les nombreux membres du projet ERNOR, par Zoom tout comme sur le terrain.

Mes remerciements s'adressent ensuite à ma famille et aux ami-es qui se demandent encore ce que j'ai fait durant ces dernières années. Merci à celles et ceux avec qui je me suis lié d'amitié lors de mon passage aux cycles supérieurs du département de Géographie. À celles et ceux qui ont remis leur thèse, je vous (re)dit bravo! À ceux et celles qui y travaillent encore, je souhaite bonne chance et bon courage.

Finalement, je me dois de remercier le soutien financier qui a permis la complétion de cette recherche : le programme MITACS, le Front de Recherche du Québec en Nature et Technologies, la Faculté des Arts et Sciences de l'Université de Montréal ainsi que le Ministère des Ressources naturelles et des Forêts.

PRÉFACE

Le présent mémoire est composé de cinq parties. L'introduction pose les grandes lignes de la problématique, identifie le site à l'étude et établit la question de recherche. Puis, suit un article scientifique qui représente la partie centrale de mon projet de recherche. La discussion générale met en lien les résultats produits dans l'article avec de nouveaux résultats. Les objectifs de recherche établis dans l'introduction y sont abordés. La conclusion retrace les grandes lignes de l'article et est suivie d'une annexe où toutes les informations supplémentaires du projet sont consignées.

L'article est intitulé *Pollen Identification Through Convolutional Neural Networks : First Application on a Full Fossil Pollen Sequence* et il sera bientôt soumis pour publication. J'en suis l'auteur principal et les coauteurs sont Jordan Paillard (conceptualisation du projet, méthodologie et validation), Marie-Pier Ménard (laboratoire et méthodologie), Thomas Suranyi (revue et validation), Pierre Grondin (supervision, financement et revue) et Olivier Blarquez (supervision, conceptualisation du projet, financement et revue). Sa présentation suit le format d'un article scientifique. Les références de l'article sont jointes à celles du mémoire. Les scripts rédigés dans le contexte de l'article sont disponibles au github.com/meddur/pollen_ai

1 Introduction

Au Québec, le territoire est caractérisé par deux grandes zones de végétation. De la frontière américaine jusqu'au 48^{e} parallèle s'étend la forêt tempérée nordique. Elle est caractérisée par une abondance des espèces décidues et thermophiles ainsi que par la faible fréquence des feux de forêt y occurrant. Au nord de la forêt tempérée nordique se trouve la forêt boréale qui s'étend jusqu'à la zone arctique. Selon un gradient sud-nord, les peuplements forestiers décidus et tempérés font place à des peuplements majoritairement conifériens. Ces forêts s'ouvrent graduellement pour faire place aux pessières et à la toundra forestière, au 58^{e} parallèle. Selon ce même gradient, les feux de forêt se font plus fréquents vers le nord et ne diminuent qu'à la toundra forestière (Saucier et al., 2009).

La zone de contact entre la forêt tempérée nordique et la forêt boréale, informellement appelée forêt mixte, est composée de deux domaines bioclimatiques (Figure 1-1). La portion sud de la forêt mixte est occupée par le domaine de la sapinière à bouleau jaune (*Betula alleghaniensis* Britt.), alors que le domaine de la sapinière à bouleau blanc (*Betula papyrifera* Marsh.) occupe la portion nord. On retrouve dans la forêt mixte une matrice forestière davantage hétérogène, où des peuplements typiquement boréaux côtoient des peuplements tempérés. Les feux y sont plus importants que dans les domaines des érablières, au sud. Dans la portion ouest de la forêt mixte, bien que le cycle de feu s'allonge depuis le petit âge glaciaire (400-200 cal. BP [Années calibrées avant le présent; *Before Present*]), il avoisine aujourd'hui les 326 ans (Bergeron et al., 2004).

Au sein du domaine de la sapinière à bouleau blanc, plusieurs espèces atteignent leur limite nordique d'aire de répartition, tel l'érable rouge (*Acer rubrum* L.), le pin blanc (*Pinus strobus* L.), le *B. alleghaniensis* et le thuya (*Thuja occidentalis* L.). Au sud, dans le domaine de la sapinière à

bouleau jaune, quelques espèces tempérées y atteignent similairement leur limite nordique d'aire de répartition, notamment l'érable à sucre (*Acer saccharum* Marsh.) (Figure 1-1). Les peuplements d'*A. saccharum* qui se trouvent à ces latitudes sont isolés de la distribution principale de l'espèce. Ils forment des érablières nordiques que l'on peut retrouver dans la portion nord du domaine de la sapinière à bouleau jaune. En situation marginale, *A. saccharum* se retrouve sur le sommet des collines (Saucier et al., 2009). Cette position topographique lui permet de bénéficier d'un climat comparativement plus chaud, de sols mésiques et d'une modeste protection face aux feux (Cyr et al., 2007).

A. Saccharum est un espèce tempérée thermophile que l'on retrouve typiquement dans les forêts de fin de succession. Elle est tolérante à la fois aux conditions ensoleillées et ombragées (Payette et al., 2018). Cette plasticité phénotypique (Nolet et al., 2008), associable à un profil généraliste, permet à *A. saccharum* d'éventuellement dominer la canopée des peuplements où on le retrouve. Les individus matures sont vraisemblablement résilients aux feux grâce à la discontinuité du combustible présent entre le sol et la canopée (Payette et al., 2018) ainsi qu'à une modeste capacité de régénération post-feu (Nolet et al., 2008). Lorsque précédée par une cohorte colonisatrice (*B. papyrifera, Pinus*) ou trans-successionnelle (*A. rubrum*, sapin baumier [*Abies balsamea* [L.] Mill.]), *A. saccharum* peut rapidement occuper la canopée d'un territoire récemment touché par une perturbation majeure (coupe à blanc, feu sévère) (Brisson et al., 1988; Nolet et al., 2008). Cette résilience – c'est-à-dire la capacité de retour à la normale suivant une perturbation majeure – peut aussi être observée en situation marginale nordique (Pilon et Payette, 2015).

Force est de constater qu'*A. saccharum* est une espèce à l'écologie complexe et ce, particulièrement en forêt mixte où elle se retrouve en compétition avec des espèces souvent mieux adaptées au climat froid ainsi qu'aux feux. Alors que plusieurs auteurs se sont penchés sur la

capacité d'*A. saccharum* à se maintenir en situation marginale nordique, il demeure encore à comprendre quand et comment ces populations satellites s'y sont installées.

Plusieurs auteurs (Carcaillet et al., 2010; Larochelle et al., 2018; Richard, 1995) soutiennent que certaines populations marginales d'espèces tempérées sont issues d'anciennes aires de répartition autrefois plus étendues vers le nord (*e.g. P. strobus, B. alleghaniensis, A. saccharum*). Ces expansions nordiques furent progressivement fragmentées par une expansion méridionale de la répartition des espèces boréales au déclin de l'optimum climatique Holocène (OCH), entre 8,000 – 5,000 cal. BP. C'est durant l'OCH, une période marquée par des conditions climatiques plus chaudes ainsi que par une biomasse accrue des espèces tempérées, que ces dernières auraient franchi leurs limites nordiques contemporaines (Bajolle et al., 2018; Blarquez et Aleman, 2016). Ce phénomène coïncide avec le mouvement de certaines espèces provenant de la forêt mixte au sein des pessières, dans la portion nord de la forêt boréale. La répartition d'*A. balsamea*, par exemple, s'étendait bien au nord de sa répartition contemporaine (Ali et al., 2008) alors que *B. papyrifera* y était plus abondant (Richard, 1995). L'OCH est suivi du néoglaciaire, une période durant laquelle le climat se refroidit dans son ensemble. Au Québec, les reconstructions paléoclimatiques identifient un refroidissement régional du climat dès 4,500 cal. BP, culminant avec le petit âge glaciaire (Bajolle, 2018; Bajolle et al., 2018). Ce climat aurait entraîné une recrudescence méridionale de la distribution de certaines espèces boréales favorisées par les températures froides (Bajolle, 2018; Carcaillet et al., 2010). Cette hausse de la prédominance des espèces boréales dans ce qui est aujourd'hui la forêt mixte aurait entrainé la fragmentation de la répartition continue de certaines espèces tempérées, notamment celle de *P. strobus* (présence régionale dès 7,600 cal. BP, déclin dès 5,000 cal. BP; Terasmae et Anderson, 1970) et de *B. alleghaniensis* (7,700 – 1,400 cal. BP; Larochelle et al., 2018).

Ces observations sont appuyées par la présence de macro-restes fossiles de *P. strobus* retrouvés dans la sapinière à bouleau blanc, à près d'une centaine de kilomètres au nord de la limite nordique contemporaine de la répartition de l'espèce (Près du lac Lili; Figure 1-1; Terasmae et Anderson, 1970). Ces macrofossiles, datés à plus de 5,000 cal. BP, témoignent de la présence locale de l'espèce durant l'OCH. La retrait de l'espèce tel qu'identifié par Larochelle et al. (dès 5,000 cal. BP) coïncide avec les températures plus froides du néoglaciaire.

Le climat plus froid engendré par la fin de l'OCH n'est pas l'unique vecteur de la recrudescence des espèces boréales. On dénote aussi un assèchement des conditions printanières dès 5,000 BP qui a résulté en une intensification de la fréquence des feux au nord de la forêt mixte (Ali et al., 2009, 2012). Ces feux plus fréquents correspondent à la chute en abondance de *T. occidentalis* (Fréchette et al., 2018) dans la forêt mixte, *d'A. balsamea* en forêt boréale (Ali et al., 2008) ainsi qu'à une baisse généralisée de la biomasse forestière (Blarquez et Aleman, 2016).

Les sites de Paillard (2018), des érablières réparties sur un transect sud-nord, retracent les mouvements d'*A. saccharum* durant l'Holocène. Deux de ces sites, l'un situé au sein de la répartition continue de l'espèce dans le domaine de l'érablière à bouleau jaune, et le second en situation marginale au nord du domaine de la sapinière à bouleau jaune, enregistrent une présence paysagère de *A. saccharum* dès 7,800 cal. BP et 5,500 cal. BP, respectivement (Lacs Fur et Chasseur, Figure 1-1). Cette intensification de l'abondance de *A. saccharum* coïncide avec une hausse de la présence du genre *Betula* qui remplace peu à peu *P. strobus* à l'échelle du paysage durant cette période. La présence de *Betula*, moins combustible que *Pinus*, aurait mené à une diminution de la propagation des feux et éventuellement à un régime de feux moins sévère. De plus, une sous-canopée dominée par des espèces décidues amplifie le potentiel migratoire des

espèces tempérées en les protégeant de la prédation herbivore, du soleil et des intempéries météorologiques (Evans et al., 2020; Solarik et al., 2020). L'apparition d'une canopée décidue de *Betula* ainsi que la chute du régime de feu aurait ainsi permis à *A. saccharum* de s'installer localement sur ces sites. Les reconstructions suggèrent un établissement local dès 5,100 BP sur le site de l'érablière à bouleau jaune et dès 4,400 BP sur le site de la sapinière à bouleau jaune. Le troisième site de Paillard (2018), situé à la limite sud de la sapinière à bouleau blanc, retrace une dynamique similaire ayant permis à *A. saccharum* de s'y installer localement durant le néoglaciaire, dès 2,700 cal. BP.

Il ne faut pas écarter la possibilité que certaines érablières nordiques pourraient plutôt être issues de colonisations récentes, durant le néoglaciaire, lorsque un régime de perturbation moins sévère l'aurait permis. Ce serait par exemple le cas du site Rémigny, une population marginale d*'Acer saccharum* située au Témiscamingue dans la sapinière à bouleau jaune (Pilon et Payette, 2015). Alors que Paillard (2018) date à 2,700 cal. BP l'arrivée locale de l'espèce 50 km au nord du site Rémigny, Pilon et Payette concluent que l'espèce ne s'y serait installée qu'il y a 200 ans. Suivant cette logique, certaines populations tempérées marginales ne seraient pas originaires d'aires de répartition nordiques ancestrales et auraient plutôt des dates d'établissement asynchrones. Ces mêmes auteurs constatent un établissement similaire de *A. saccharum* lors de leurs analyses botaniques des charbons fossiles retrouvés dans les érablières marginales des sites Rivière-Éternité (où l'arrivée locale de l'espèce remonte minimalement à 1,970 cal. BP) et Forillon, où leur arrivée se situe entre le 17^{e} et 18^{e} siècle CE (ère commune; *Common era*) (Payette et al., 2018).

Aujourd'hui, face à un réchauffement climatique durant lequel les espèces forestières voient leur optimum climatique migrer vers le nord (Chen et al., 2011; Pitelka, 1997), il est crucial d'étudier

les populations marginales nordiques en vue de comprendre les dynamiques régissant la migration et la persistance des espèces tempérées en milieu boréal.

Les milieux forestiers boréaux présentent des propriétés inhibitives à l'établissement de *Acer saccharum*. Ces effets prioritaires (*priority effects*; Solarik et al., 2020) – soit la modification de la disponibilité des nutriments, du pH, et d'autres propriétés du sol – freinent la migration d'*A. saccharum* (Collin et al., 2018; Solarik et al., 2020). Au même titre que bien d'autres espèces tempérées, *A. saccharum* fait donc face à une pression climatique croissante les poussant à migrer dans des environnements nordiques colonisés et peu propices à leur établissement (Solarik, 2017).

D'autant plus, alors que les régions boréales s'apprêtent à enregistrer un rallongement de la saison des feux, la sévérité du régime de feu est appelée à hausser durant les prochaines années (Wotton et al., 2010). Au vu de cette perspective, il est important d'améliorer notre compréhension des érablières nordiques afin de nous assurer de la survie de ces espèces et de la conservation de la biodiversité des milieux forestiers. Pour ce faire, nous avons étudié une érablière nordique située aux abords du lac Bélanger, en Haute-Mauricie, (47.4760 N, -75.1773 O, Figure 1-1), au sud de la frontière séparant le domaine de la sapinière à bouleau blanc de celui de la sapinière à bouleau jaune. Cette érablière est formée d'érables à sucre matures dominant la canopée accompagnés de bouleaux jaunes.

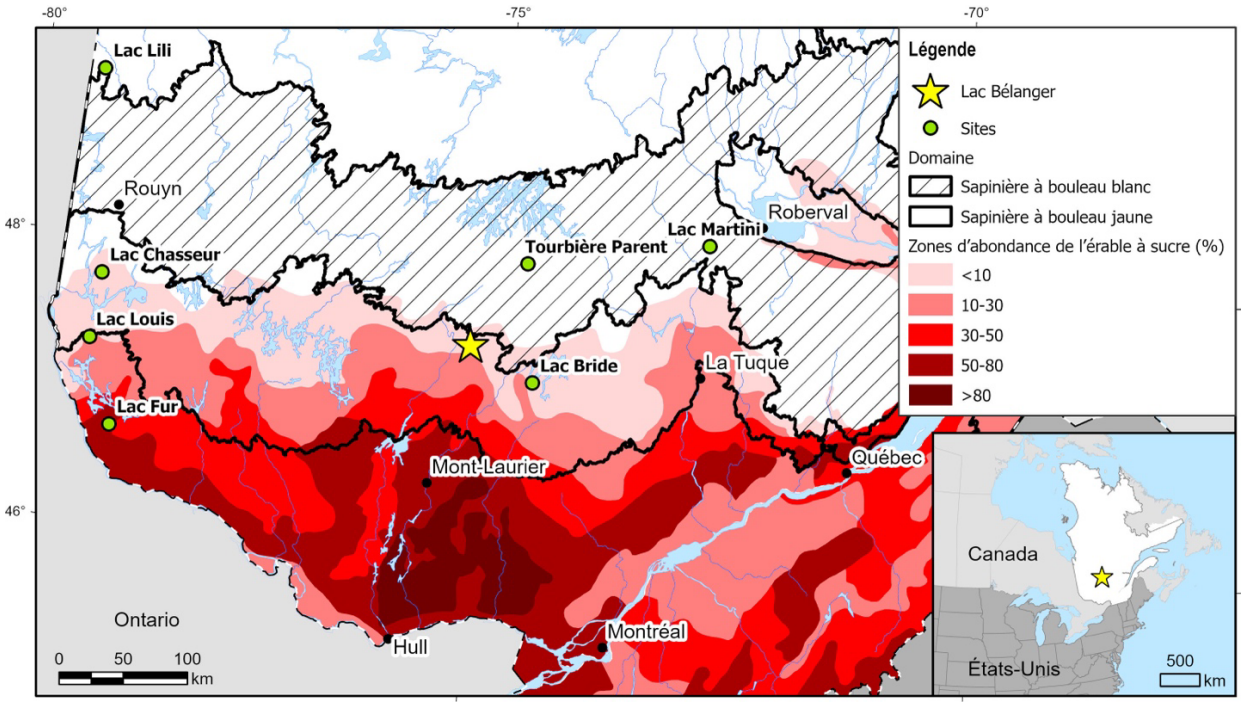

Figure 1-1 – Carte de la zone à l'étude. L'érablière du lac Bélanger se trouve au sud de la délimitation entre le domaine des sapinières à bouleau blanc et des sapinières à bouleau jaune. En rouge : abondance d'A. saccharum. En vert : sites où ont été menées des études paléoécologiques, notamment Bajolle (2018), Larochelle et al. (2018), Paillard (2018), Richard (1993) et Vincent (1973). Carte produite par Véronique Poirier (Ministère des Ressources naturelles et des Forêts du Québec, 2023).

À travers l'étude paléoécologique des dynamiques passées de *A. saccharum* au lac Bélanger, ce projet de recherche a comme objectif de déterminer quand et sous quelles conditions les érablières nordiques ont-elles pu s'établir à de latitudes si élevées au sein du domaine de la sapinière à bouleau jaune. Je tenterai de déterminer si l'érablière à sucre du lac Bélanger est soit i) un vestige de la dynamique d'expansion-rétraction durant l'Optimum Climatique Holocène ou ii) un établissement plus récent datant du néoglaciaire. À ces fins, l'article qui suit présente une analyse paléoécologique de la végétation du lac Bélanger. Pour ce faire, j'y propose un modèle d'intelligence artificielle permettant la classification des pollens fossiles extraits des sédiments lacustres du lac Bélanger. Au fil de l'article, je m'attarde sur la performance du modèle et je compare ses résultats à ceux obtenus par palynologie « traditionnelle ».

2 Article

Pollen identification through convolutional neural networks: first application on a full fossil pollen sequence

Médéric Durand[1], Jordan Paillard[1a], Marie-Pier Ménard[1b], Thomas Suranyi[1,2,c], Pierre Grondin[3,c,d], Olivier Blarquez[1,a,c,d]

[1] Département de Géographie, Université de Montréal, Montréal, Québec, Canada

[2] Laboratoire Chrono-Environnement, UMR 6249 CNRS, Université de Franche-Comté, Besançon, France

[3] Direction de la recherche forestière, Ministère des Ressources naturelles et des Forêts, Québec, QC, Canada

Déclaration d'apport original et indépendant :

Cet article est un manuscrit représentant la majorité des travaux de recherche que j'ai entrepris lors de ma maîtrise en Géographie à l'Université de Montréal. J'en suis l'auteur principal : outre les apports des coauteurs annotés ci-bas, j'ai conçu, entrepris et écrit l'entièreté du travail nécessaire à la rédaction de cet article. En date de juin 2023, cet article est en voie de soumission.

[a] Méthodologie – Conceptualisation

[b] Méthodologie – Travaux de laboratoire

[c] Manuscrit – Révision et correction

[d] Supervision

2.1 Abstract

The automation of pollen classification has seen vast improvements in the past years, with Convolutional Neural Networks coming out as the preferred tool to train models. Still, only a small portion of works published on the matter address the classification of fossil pollen. Fossil pollen is commonly extracted from organic sediment cores and are used by paleoecologists to reconstruct past environments and their evolution through time. The automation of fossil pollen classification would allow paleoecologists to save both time and money while reducing bias and uncertainty. Since machine learning models are usually trained using labelled fresh pollen associated with many different species, there exists a gap between the training data and target data. We propose a method for a large-scale fossil pollen classification workflow. Our proposed method employs an accelerated fossil pollen extraction protocol and Convolutional Neural Networks trained on the labelled fresh pollens of the species most commonly found in Northeastern American organic sediments. We first test our model on fresh pollen and then on a full fossil pollen sequence totalling 196,526 images. Our model achieved an average per class accuracy of 91.2% when tested against fresh pollen. However, we find that our model does not perform as well when tested on fossil data. While our model is overconfident in its predictions, the general abundance patterns remain consistent with the traditional palynologist IDs. Although not yet capable of accurately classifying a whole fossil pollen sequence, our model serves as a proof of concept towards creating a full large-scale classification workflow.

2.2 Introduction

The scientific field of palynology is the study of spores and pollen grains. Through the analysis of discriminating morphological features, palynologists can associate microscopic pollens to their parent species. For decades, palynology has been a useful method in numerous disciplines including honey production and allergen forecasting through the use of airborne pollen (Louveaux et al., 1978; Suanno et al., 2021). Moreover, it has been of significant importance as a tool in the reconstruction of past environments, or paleoecology. The identification of fossilised pollen grains extracted from a sediment core allows paleoecologists to study past vegetation communities and their evolution through time (Birks et Birks, 1980). Traditionally, this method involves a highly trained analyst identifying pollens under a light microscope. As between 300 and 500 pollens need to be identified within a sample for it to be statistically significant (Birks et Birks, 1980), palynology is generally understood to be a long and tedious process.

Achieving automation in palynology could solve many problems besetting the field – it could greatly accelerate the identification process while reducing the bias and uncertainty brought on by an analyst. This is because pollen grains are often morphologically similar, especially if belonging to closely related species. For example, a 2014 study highlighted that an analyst's identification consistence between *the same pollen sample slide analysed twice* could range from 32.5% to 87.5% (Mander et al., 2014). All the more, expecting consistent results from different analysts should not be expected (MacLeod et al., 2010). Automating palynology would help guaranteeing a degree of consistence in both an analyst's work and between the work of different analysts. Furthermore, by decreasing analysis time, automating palynology could result in more samples being analysed. In the context of palyno-paleoecology, increasing the number of samples along a

single sediment core would result in a higher temporal resolution. Analysing fossil pollen sequences at a high resolution would allow paleoecologists to quantify ecological processes more accurately. In the hypothetical case of a species' pollen suddenly disappearing from pollen assemblages, a high temporal resolution analysis could help quantifying the species' rate of decline. Ideally, a classification algorithm would be combined with an automated slide scanner, which would allow for a large-scale classification workflow of numerous images along a sediment core.

In the past years, considerable effort has been spent automating pollen grain identification, mainly using deep learning algorithms (Bourel et al., 2020; Geus et al., 2019; Punyasena et al., 2022). Images of pollen grains are first captured either manually by cropping the pollen under a light microscope or automatically with the use of a slide scanner (Pedersen et al., 2017; Sevillano et al., 2020). Then, deep learning models are trained using those images in order to classify other similar looking pollen. For a time, the main focus of papers regarding this matter revolved around optimizing feature selection and extraction – generally understood as a model's capacity to pick out a pollen grain's important morphological features (size, texture, symmetry, number of pores, exine thickness, etc…) and to identify which of those features are discriminatory. The discriminatory features, once properly weighted, are then used to train a classifier. Holt et al. (2011), Kaya et al. (2013), Lagerstrom et al. (2013) and Nguyen et al. (2013) all proposed such pollen classification models featuring varying degrees of user input in the feature selection and extraction phases. In recent years, the advent of convolutional neural networks (CNNs), a type of deep learning network, has permitted the automatic extraction and selection of relevant features without human supervision (Alzubaidi et al., 2021). This has brought on a number of very reliable

pollen classification models (Bourel et al., 2020; Daood et al., 2018; Dunker et al., 2020; Khanzhina et al., 2018; Punyasena et al., 2022; Sevillano et al., 2020; Sevillano et Aznarte, 2018), each of them tailored to their own needs.

Despite all of this work, there are no deep learning studies that trained a CNN that is adapted to the large-scale classification of fossilised pollen. To our knowledge, there are two reasons why this is the case: i) most published deep learning algorithms were trained using clean pollen samples, usually fresh airborne pollen or extracted from honey. However, fossilised pollens are often bent, broken, covered by debris or simply clumped together. They also show no trace of any cellulose content, usually visible in fresh pollens. Since the training data must be representative of the target data, this is an issue. New methods that take into consideration the specificity of fossil pollens need to be integrated into the research. Ii) palynologists that did train their algorithms using fossilised pollen, did so by manually cropping the pollens from a noisy background and labelling them, thus removing microscopic minerals and other non-pollen palynomorphs (NPPs) from the final images (Bourel et al., 2020; Geus et al., 2019; Sevillano et Aznarte, 2018). While manually cropping pollens avoids a problematic step in automated pollen recognition, it is time intensive and so is better suited for small-scale and precise classification problems. Large-scale automation implies the use of an automated slide scanner and the inevitable presence of NPPs and images of large pollen clumps in the dataset.

This paper aims to train a CNN adapted to the classification of images of fossilised pollens found in Québec organic sediment cores and captured using an automatic slide scanner. We want our

CNN (henceforth referred to as 'the model') to be adapted to a large-scale workflow of fossil pollen classification – Thus, we present a fossil pollen extraction method that aims to minimize the time spent per sample in the lab.

We choose to further evaluate our model by testing it on a fossil pollen image dataset (Table 2-1) (*i.e.* testing our model on data originating from a different source than the data used to train the model). This independent dataset is composed of fossilised pollen extracted from the sediment core of lac Bélanger, situated in central Québec (Figure 2-1).

Tableau 2-1 : Dataset glossary: This reference table indicates where the data comes from and what it is used for. Each dataset falls under either the CNN dataset (Non-fossil images used to train, test, and validate the model) or the fossil image dataset (Fossil object images captured using the Classifynder automated slide-scanner; used to further test the CNNs)

Dataset	Description	Labeled	# images	Relevant Methods
CNN dataset	Images used to train and test the CNNs; Either fresh pollens or from the ref. collection	Y	16,331	2.2, 2.3
Training dataset	Used to train the CNNs	Y	12,248	2.2, 2.3
Testing dataset	Used for the first round of testing (Figure 2-5)	Y	2,450	2.2, 2.3
Validation dataset	Used to validate training, to compute the negative loss likelihood metric (NLL) and to calibrate the CNNs	Y	1,633	2.3
Full fossil image dataset	Classyfinder slide-scanner images taken from the lac Bélanger fossil sediment core; Used to plot the high-resolution model pollen diagram (Figure 2-8)	N	196,562	2.4; 2.5
Fossil testing dataset	30 samples taken from the Fossil image dataset; The Classyfinder slide-scanner images were visually labelled by a palynologist; Used for the second round of testing (Figure 2-6 ; Figure 2-7).	Y	20,151	2.5

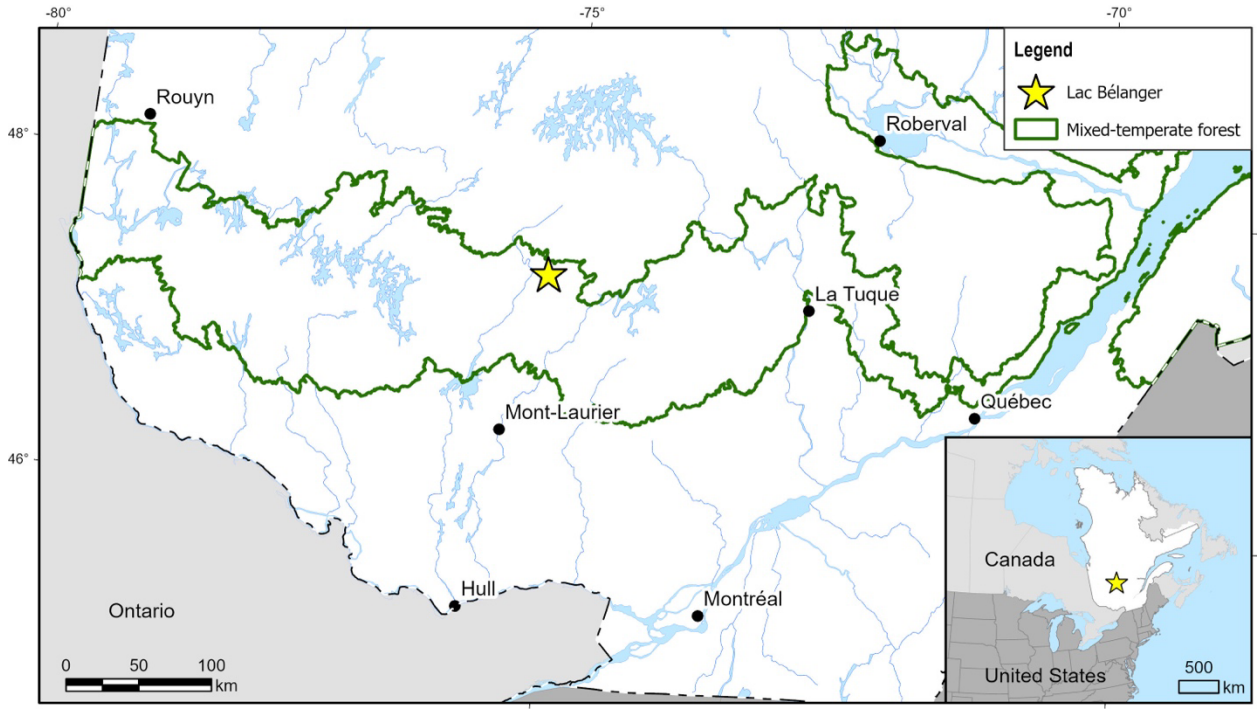

*Figure 2-1 – Map of the study site. Lac Bélanger, whose organic sediment core is used to generate the full fossil dataset. It is located within Québec's mixed-temperate forest, which is comprised of both temperate forest species (*P. strobus, A. saccharum, Quercus, B. alleghaniensis*) and stress-resistant boreal species (*P. banksiana, A. balsamea, Picea, B. papyrifera*).*

The fossil pollen grains were digitized using an automatic slide scanner. Using this fossil dataset, a first palynologist/model comparison is done using 20,151 unlabelled slide-scanner images distributed along 30 samples – assessing a model's accuracy compared to a human counterpart is best done using the same material (Holt et Bennett, 2014). We then compare the full high-resolution pollen diagram (created using 196,562 unlabelled images distributed among 271 samples from the full fossil image dataset) to a low temporal resolution pollen diagram created using traditional palynology. We hypothesize that while a drop in model accuracy might be observed, the model's predictions will resemble results obtained through traditional fossil

palynology. We believe that the tendencies in pollen abundance observed between the two methods will be consistent with one another.

2.3 Methods & material

2.3.1 General approach

The CNN dataset (the training, testing and validation data) is constructed using both reference slides and fresh pollen. Inspired by the multi-CNN method presented in Bourel et al. (2020), we train multiple small CNNs and link them hierarchically into a full network – the model Figure 2-2. This model allows for a classification to be stopped at a higher taxonomical level. By doing so, an uncertain model prediction can result in a pollen being classified at the genus level rather than down to the species level. We choose to limit the number of different classes the model is trained on to 14. These include: the balsam fir (*Abies balsamea* [L.] Mill.), red maple (*Acer rubrum* L.), sugar maple (*Acer saccharum* Marsh.), mountain alder (*Alnus crispa* Aiton), grey alder (*Alnus rugosa* L.), the birch genus (*Betula*), hazelnut (*Corylus cornuta* Marsh.), the eucalyptus genus, often used as exotic markers (*Eucalyptus*), the juniper-thuja morphological type class (*Juniperus communis* L. and *Thuya occidentalis* L.), the spruce genus (*Picea*), jack pine (*Pinus banksiana* Lamb.), white pine (*Pinus strobus* L.), the oak genus (*Quercus*) and an NPP/minerals class (Figure 2-2). Including the intermediate hierarchical classes, an image can be classified in one of 23 classes. After testing the model on the CNN training dataset, we test the algorithm using the lac Bélanger's fossil testing dataset.

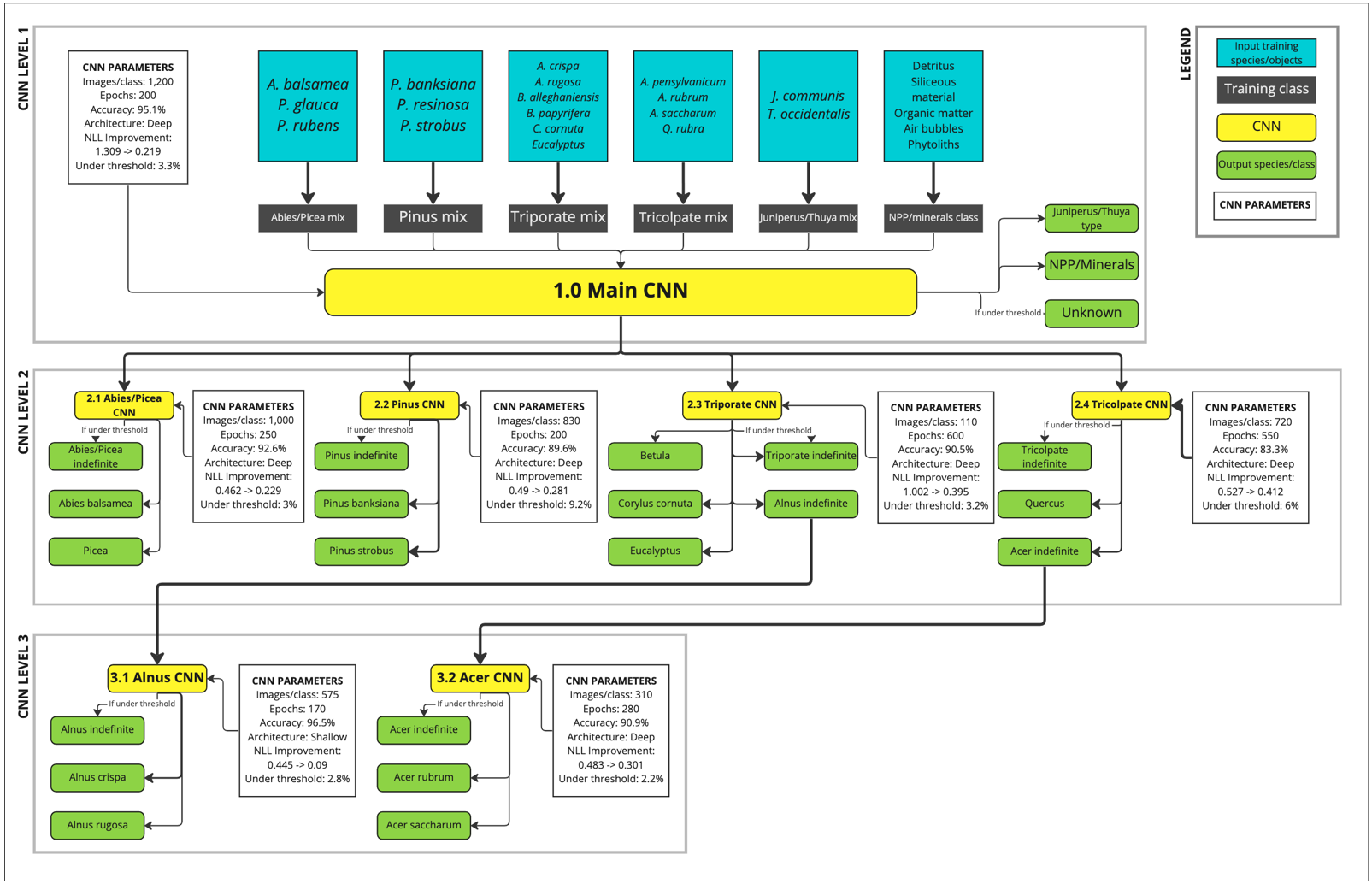

Figure 2-2 – Model flowchart. It shows the composition of the training data (blue squares), how the seven different CNNs are hierarchically joined in a full network (yellow squares and arrows), their relevant training information (white squares) and their outputs (green squares). In order to be classified, an image would be fed from the top (Level 1; Main CNN) and would potentially travel down to the third level (Either Alnus CNN or Acer CNN). The "Images/class" parameter accounts for all of the corresponding training, testing and validation images. The "Under threshold" metric corresponds to the proportion of test images that fell under the 0.7 confidence threshold during evaluation i.e. the proportion of the test set that was classified as "unknown" (μ: 4%).

2.3.2 Datasets and image acquisition

We assembled a complete dataset consisting of 16,331 images of pollen grains belonging to 18 different species (classes) usually found within North-Eastern American Holocene organic sediment cores – the CNN dataset. As is usually the case in traditional palynology, certain classes whose pollens are morphologically similar were combined into a single class, bringing down the total amount of pollen classes the algorithm was trained on to 13 (Table 2-2).

Tableau 2-2 : Information on the training dataset. Each pollen taxa (Species) makes part of a Class, usually made up of pollen of a similar morphological group. For each taxa, the source, their additional laboratory treatment (if any) and their number of grains is tallied. The training dataset is fed into the model in order to train it (Figure 2-2).
**While not of triporate morphology, Alnus pollens have been assigned to the triporate morphological group in order to streamline the classification process*

Morphological type	Species	Class	Source	Additional lab treatment	Total grains
Aporate	*Juniperus communis* L.	Juniperus/Thuya type	Reference collection		1301
Aporate	*Thuya occidentalis* L.	Juniperus/Thuya type	Fresh		194
Tricolpate	*Acer pensylvanicum* L.	Tricolpate mix; Acer	Reference collection	Acetolysis	251
Tricolpate	*Acer rubrum* L.	Acer; Acer rubrum	Fresh	Acetolysis	1272
Tricolpate	*Acer saccharum* Marsh.	Acer; Acer saccharum	Fresh	Acetolysis	302
Tricolpate	*Quercus rubra* L.	Tricolpate mix; Quercus	Reference collection		1856
Triporate	*Betula alleghaniensis* Britt.	Triporate mix; Betula	Fresh	Enzymes	295
Triporate	*Betula papyrifera* Marsh.	Triporate mix; Betula	Reference collection		675

Triporate	*Corylus cornuta* Marsh.	Triporate mix; Corylus cornuta	Fresh	Acetolysis	1777
Triporate	*Eucalyptus* sp.	Triporate mix; Eucalyptus	Reference collection		1531
Triporate*	*Alnus crispa* Aiton	Triporate mix; Alnus; Alnus crispa	Fresh		773
Triporate*	*Alnus rugosa* L.	Triporate mix; Alnus; Alnus rugosa	Fresh		1931
Vesiculate	*Abies balsamea* (L.) Mill.	Abies/Picea mix; Abies balsamea	Reference collection		1183
Vesiculate	*Picea glauca* (Moench) Voss	Abies/Picea mix; Picea	Fresh	Enzymes	344
Vesiculate	*Picea rubens* Sarg.	Abies/Picea mix; Picea	Fresh	Enzymes	532
Vesiculate	*Pinus banksiana* Lamb.	Pinus mix; Pinus banksiana	Reference collection	50% enzymes; 50% acetolysis	923
Vesiculate	*Pinus resinosa* Aiton	Pinus mix; Pinus banksiana	Reference collection		269
Vesiculate	*Pinus strobus* L.	Pinus mix; Pinus strobus	Fresh	Enzymes	922

The pollen grains composing the CNN dataset originated from different sources. Some were found in the Université de Montréal's pollen refence collection. The pollens from classes that were absent from the collection were instead harvested directly from tree flowers and cones during each species' flowering period (Table 2-2). They then were stored in 70% proof ethanol tubes until further treatment. The dispersing effect of ethanol accentuated the separation of the pollen grains from the flowers and cones.

Each sample was then submerged in a potassium hydroxide solution (KOH 20%) under heat for 20 minutes before being washed with water and filtered through a 150 µm mesh. When put under a light microscope, certain species' pollen grains still showed visible cellulose content. In order to clear the cellulose contained within the grains, two different methods were used. We followed an enzyme-based method to successfully clean out the grains of *B. alleghaniensis, P. glauca, P. rubens* and *P. banksiana* (O'Keefe et Wymer, 2017). This was achieved by using an equal part pectinase to cellulase ratio (0.1 g), 10 ml distilled water and a 10 ml citrate buffer, bringing the final pH to 6.5. The remaining species' grains still containing cellulose were cleaned through acetolysis (Table 2-1).

Prior to the pollen solution being mounted on the slides, the 70% proof ethanol was emptied from the tubes and replaced by 90% proof ethanol in order to accelerate evaporation. The slides were then mounted using a warm glycerin jelly solution and given a few minutes for the ethanol to evaporate. The slides were then sealed and cooled off in order to let the solution and pollens set.

The images were acquired using Veritaxa's Classyfinder, an automated slide scanner, at a 40x magnification under dark-field illumination. The pollen was automatically identified through the use of morphological criteria input by the user. Using the Classyfinder's software, the final images were generated as a Z-stack, fusing the different images of the grain taken along the depth at a 1(one) µm interval (Pedersen et al., 2017) (Figure 2-3). Using the same image capture method, a 14^{th} class was added to the CNN dataset, comprising of 1,375 images of various NPP/minerals that can be found in lake sediment pollen slides, namely clay particles, chironomid, phytoliths and air

bubbles, all mistakenly captured by the Classyfinder microscope. As a means to standardize the data and improve training performance, the CNN dataset was then transformed to grayscale and rescaled to 128x128 pixels. 75% of the CNN dataset was randomly selected to create the training dataset. The testing dataset was constructed using 15% of the CNN dataset, while the validation dataset was formed using the remaining 10%.

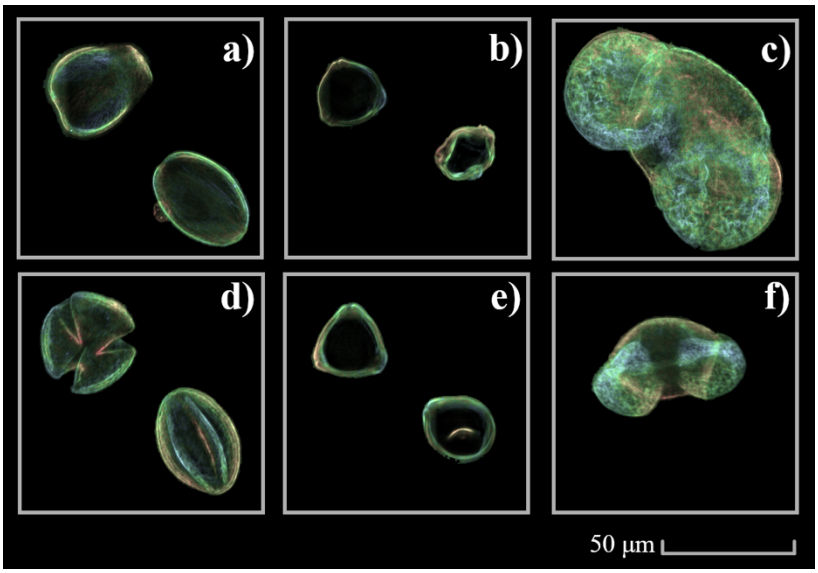

Figure 2-3 – Different pollen taxa as captured by the Classyfinder slide scanner. Morphological type is indicated between parentheses: a) A. rubrum *(tricolpate); b)* B. alleghaniensis *(triporate); c)* P. strobus *(vesiculate); d)* A. saccharum *(tricolpate); e)* C. cornuta *(triporate); f)* P. banksiana *(vesiculate)*

2.3.3 Model conception and image classification

The deep learning project was coded using Python. The training was done using the CNN training dataset (Table 2-1), employing both the Keras and Tensorflow APIs. Following the method found in (Bourel et al., 2020), multiple CNNs were trained and hierarchically assembled, forming a "multi-CNN" system. Each of those seven CNN was trained on its own subset of pollen classes according to their morphological similitude (Figure 2-2).When fed into the system, the input data is either classified as belonging to a particular pollen class, sent to a CNN of a higher hierarchical

level, or, if its prediction fails to reach a confidence threshold, is dropped out of the classification process. Drop-outs remain accounted for and are registered as belonging to their parent class, *e.g.,* having reached the Acer CNN, an *A. saccharum* pollen failing to clear the confidence threshold would still be counted as belonging to the *Acer* genus, as a real palynologist would. Considering that morphologically similar pollen grains generally belong to taxonomically related species, the class composition and total amount of CNNs has been determined through morphological similitude.

Since the training of a deep learning algorithm using imbalanced data may result in the overfitting of one of its classes, each CNN's corresponding dataset size was limited to the number of images present in least populated class (Figure 2-2). As is commonly done for the training of image classification models, our model used data augmentation techniques during training. This module allowed the simultaneous generation of 'new' training images during each iteration (batch sent through the network), *de facto* increasing the total amount of training data available for each CNN. These 'new images' were generated by randomly applying rotations (0-45°), shearing (0-15%) and lowering luminosity (0-20%).

The CNNs' common core architecture comprised of 6 trained layers (Figure 2-4). The main elements of a CNN are present: two convolutional layers with a ReLU activation function are followed by a single max pooling layer, doubling the filter size and connecting to two additional convolutional layers until the fully connected layer is reached at the top. For a relatively recent review of deep learning concepts and terms, see (Alzubaidi et al., 2021).

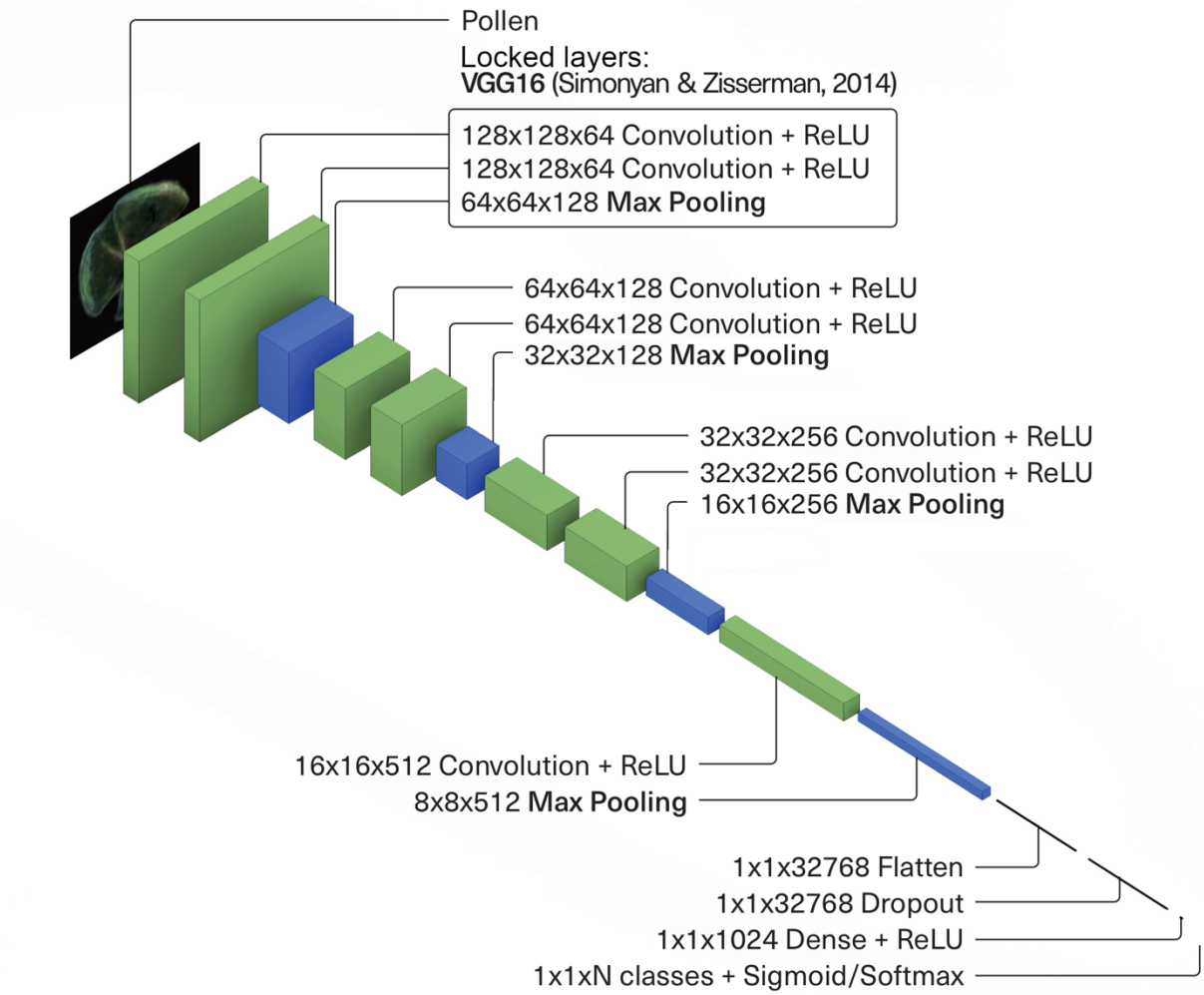

Figure 2-4 – Architecture of the Convolutional Neural Networks. The first three layers present after the inputs (left to right) are transfer learning layers. The next six layers represent the common core, present in all seven networks. The following two layers were present only in the deep architecture networks. For the Alnus CNN, a shallower model was used wherein the last convolutional and max pooling layers are removed. The fully connected layer is comprised of the last four layers. See Alzubaidi et al. (2021) for a review on the terms and layers discussed in this paper.

At the bottom of each model, two convolutional layers and a max pooling layer were imported from the VGG16 pre-trained image classification network (Simonyan et Zisserman, 2015). This

process, called transfer learning, is employed to make use of another network's pre-trained layers in order to increase the feature extraction capacity of our own models. The layers imported from the VGG16 neural network were taken from its first block, situated at the bottom, wherein the layers were trained to extract basic features. Relying on transfer learning instead of our own models' low level randomized feature extraction allows for deeper feature processing in our models' subsequent convolutional layers. This technique was shown to be effective in palynological image classification problems (Daood et al., 2018; Sevillano et Aznarte, 2018). A dropout layer was inserted as the beginning of the fully connected layer, dropping 50% of each batch's tensors, lowering the overfitting chances in the process. The fully connected layer is ultimately activated using a softmax activation function.

In accordance with Guo et al. (2017), the softmax output tensors – the predictions – were transformed using temperature scaling, a variant of Platt scaling. By scaling the output logits by the parameter T ($T>0$), temperature scaling calibrates the models' outputs by lowering the prediction confidence without affecting the models' accuracy. Employing the validation dataset images, each model's T was calculated using the negative log likelihood (NLL) and the validation loss metric prior to predicting. A 0.7 threshold was applied to the prediction outputs. Each image whose prediction fell under this threshold was assigned the *Unknown* label and dropped out of the model. If the image reached a classification level higher than 1 before falling under the threshold, it was instead marked as an indefinite object belonging to its parent class before dropping out of the model.

Other than dataset size and temperature *T*, using a multi-CNN approach has allowed us to tailor fit certain parameters according to the available data. Namely, each model was trained using its own optimized number of epochs (Figure 2-2). Furthermore, two different model architectures were used to train the seven CNNs: a shallow and a deep architecture (the latter can be visualized on Figure 2-4). Both architectures share the same common core, batch size and input size. The shallow architecture was only used to train the Alnus CNN (Figure 2-2), since its input data tended to overfit rapidly. Used to train the remaining six CNNs, the deeper architecture adds both a single additional convolutional layer and a max pooling layer, thus doubling the number of output filters in the fully connected layer. As with each model's chosen number of epochs, the various parameters and their optimal values, including the choice of architecture, *T*, batch size and transfer learning layers, all depend on the dataset size and overall image complexity and thus have been determined experimentally.

2.3.4 Fossil pollen extraction

In order to steer training accuracy and to optimize parameter tuning, the models have been tested using data from the testing dataset. As shown in section 2.3.2, the testing dataset was generated using fresh pollens, similarly to the training dataset. To further test the model, a fossil image dataset was created using fossil pollens extracted from lac Bélanger's sediments. The purpose of this second round of testing is to effectively test the model using images of fossilized pollen which have undergone various degrees of weathering and decay.

Lac Bélanger is located in central Québec (47.476045, -75.177318) and was sampled in the summer of 2017 (Figure 2-1). With an annual average temperature close to 0°C and annual precipitations averaging 1,000mm, it is situated within Québec's mixed-temperate forest. While regionally *A. balsamea* and *B. alleghaniensis* usually make up the dominating stands, lac Bélanger is characterized by a bordering *A. saccharum* stand, where it reaches its northern distribution limit. Its extracted sediment core measures 8.1 meters. 10 samples have been dated using radiocarbon dating techniques. Its basal age is 9,978 (±290) calibrated years before present (cal. BP). Its temporal resolution averages 12.4 years/cm.

271 levels were chosen and sampled along the sediment core's depth at an interval averaging 3 cm. Pollens composing the fossil image dataset have been extracted from the lacustrine sediment samples using a different method than those extracted in section 2.3.2. The traditional method (Fægri et al., 2007) relies on acidic treatments to dissolve leftover cellular content (acetolysis) and siliceous material (hydrofluoric acid), with the unintended side effect of further damaging the pollen grains. Moreover, only a small portion of the CNN training dataset has undergone acetolysis. While a human palynologist would see little to no problem discriminating pollens from NPP/minerals, especially siliceous, dispensing with the removal of such content would put an unnecessary strain on both the Classyfinder software and the model. Furthermore, since the usage of an automated pollen classification method is hugely beneficial to large scale work, minimizing the time spent per sample is crucial. Considering these constraints, the development and usage of a new method was necessary.

One (1) cm^3 was sampled from each sediment sample into a 10ml tube. A known quantity of an exotic marker solution of *Eucalyptus* (15,319 ± 1,975) was added to each tube. Exotic pollen markers are used in palynology to calculate pollen influx (n/cm^2/year). Consequently, it is necessary for *Eucalyptus* pollen to be in the training data. Each tube was then filled with a potassium hydroxide solution (KOH 20%) and immersed in an ultrasonic bath filled with boiling water for 20 minutes before being washed with distilled water. This has the effect of removing humic acids and deflocculating the pollen grains from themselves and other organic particles. Each pollen was then filtered through a 150 µm mesh and a 15 µm mesh. The content that had not filtered through the 15 µm mesh was then collected, put in a 10 ml tube and submerged in a heavy liquid of 1.7 density (sodium polytungstate). Detailed in Campbell et al. (2016), this method allows for a density based separation of the pollen solution from the siliceous particulates. It has also been shown to be effective with gyttja and other organic-rich sediment (Nakagawa et al., 2008). After mixing the tubes' content, they were centrifugated twice in a row. The first centrifugation ran at 1,500 RPM for a duration of 5 minutes, while the second ran at 2,000 RPM for the same duration. The process results in a segmentation of the 'traffic' within the tubes: the lower speed centrifugation causes the less dense organic matter to float up while the faster centrifugation ultimately brings the denser siliceous material downwards. Using a pipette, the floating pollens were then collected and filtered through the 15 µm mesh. The material that did not filter through the mesh was then gathered and stored in 70% proof ethanol until further treatment. This method allows for the treatment of up to 30 samples in an 8 hour day.

2.3.5 Fossil pollen testing dataset

The 271 pollen slides were then mounted and the images captured similarly to the ones in section 2.3.2. These 196,526 unlabelled images form the fossil image dataset and were plotted as a full pollen diagram featuring pollen biozones computed using a statistical cluster analysis (CONISS) and the broken-stick zonation method (Bennett, 1996). 30 samples were chosen from the fossil image dataset at an interval averaging 30 cm, forming the fossil testing dataset. This dataset's 20,151 slide-scanner images were visually classified – but not individually labelled – by a human palynologist into the same output classes offered by our model, with the exception of *Alnus* images: since the image quality was too low, images visually classified as *Alnus* were not further classified into either the Alnus crispa or Alnus rugosa class. Pollens that were not present in the model (*e.g. Larix laricina* [Du Roi]*, Tsuga canadensis* [L.]) were instead classified as *Unknown*. This was also the case with pollens that couldn't be properly identified because of the low image quality. Triporate or tricolpate pollens that were not used to train the model were still classified as such (e.g. *Fagus grandifolia* [Ehrh.] were classified as belonging to the Tricolpate class).

Identifying two-dimensional Z-stack images of pollens considerably limits the potential for both precision and certitude than doing so through a light microscope. That being said, we believe that this approach has resulted in consistent identifications and that it was the only way to isolate the model's "own" error – by bypassing any bias and errors introduced by the Classyfinder automated microscope during image capture.

2.4 Results

2.4.1 Training results

Our model has a 91.2% average per-class accuracy (APC) (Figure 2-5). The top-level classifier has a 95.1% APC. The mid-level classifiers show lower accuracies: the Abies/Picea CNN yields 92.6% APC; the Pinus CNN 89.6% APC; the Triporate and Tricolpate CNN yield 90.5% and 83.3%, respectively. At the third taxonomic level, the Acer CNN has an APC of 90.9%, while the Alnus CNN tests at a 96.5% APC. The average proportion of test images whose prediction fell under the 0.7 threshold is 4%. Using temperature scaling, all the models have been calibrated. This is visible in the decreasing NLL values shown in Figure 2-2 , showing both pre and post calibration NLL values. The models that benefited the most from calibration were the two non-binary CNNs.

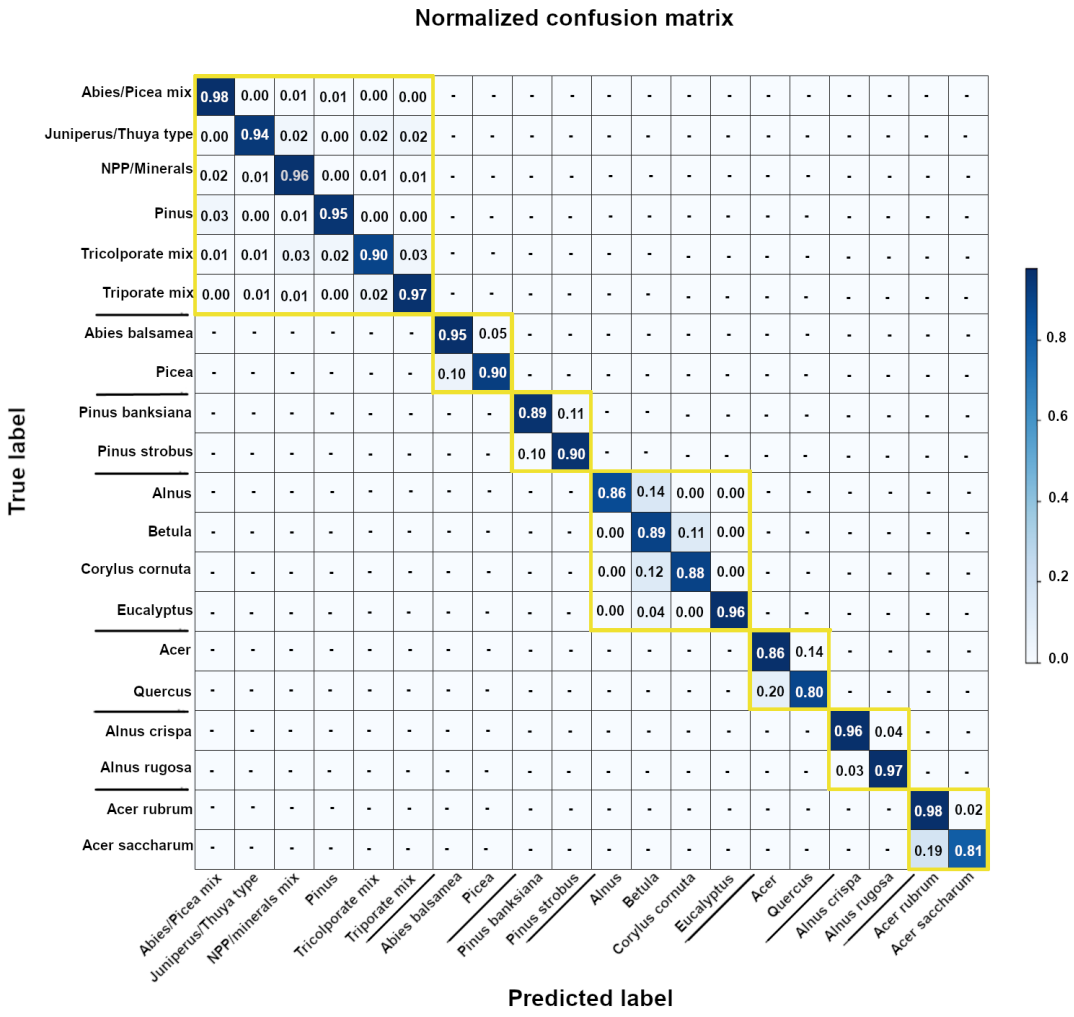

Figure 2-5 - The confusion matrix showing the training accuracy of our seven models when tested on the test dataset. The models are arranged in hierarchical order from the top-left towards the bottom-right. The data has been normalized.

2.4.2 Comparison with the fossil testing dataset

We used a set of images independent from the training process to evaluate the model's accuracy. These images come from the fossil testing dataset and were labelled by a palynologist without the use of a light microscope (*i.e.* the palynologist used the Classyfinder slide scanner's two-dimensional Z-stack images). These predictions were then compared to the model's predictions

(Figure 2-6). Scatterplots and their respective linear correlation curves were plotted in order to illustrate each class's correlation to the fossil testing dataset (Figure 2-7).

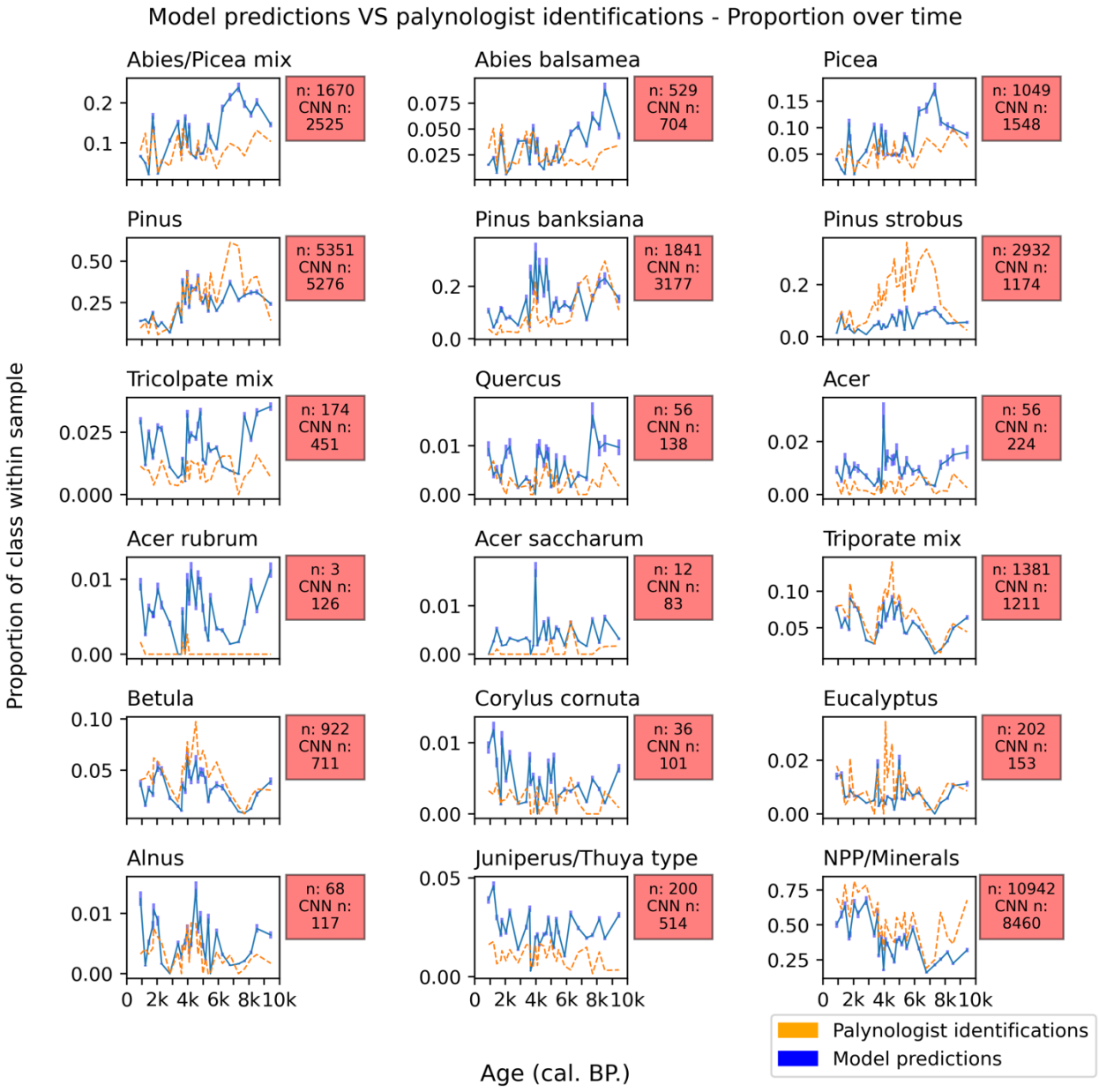

Figure 2-6 - Proportion over time of each possible output class, minus Alnus crispa and rugosa. Both the observed n and CNN predicted n are next their class plot. The time series corresponds to 30 carbon-dated samples analysed along lac Bélanger sediment core.

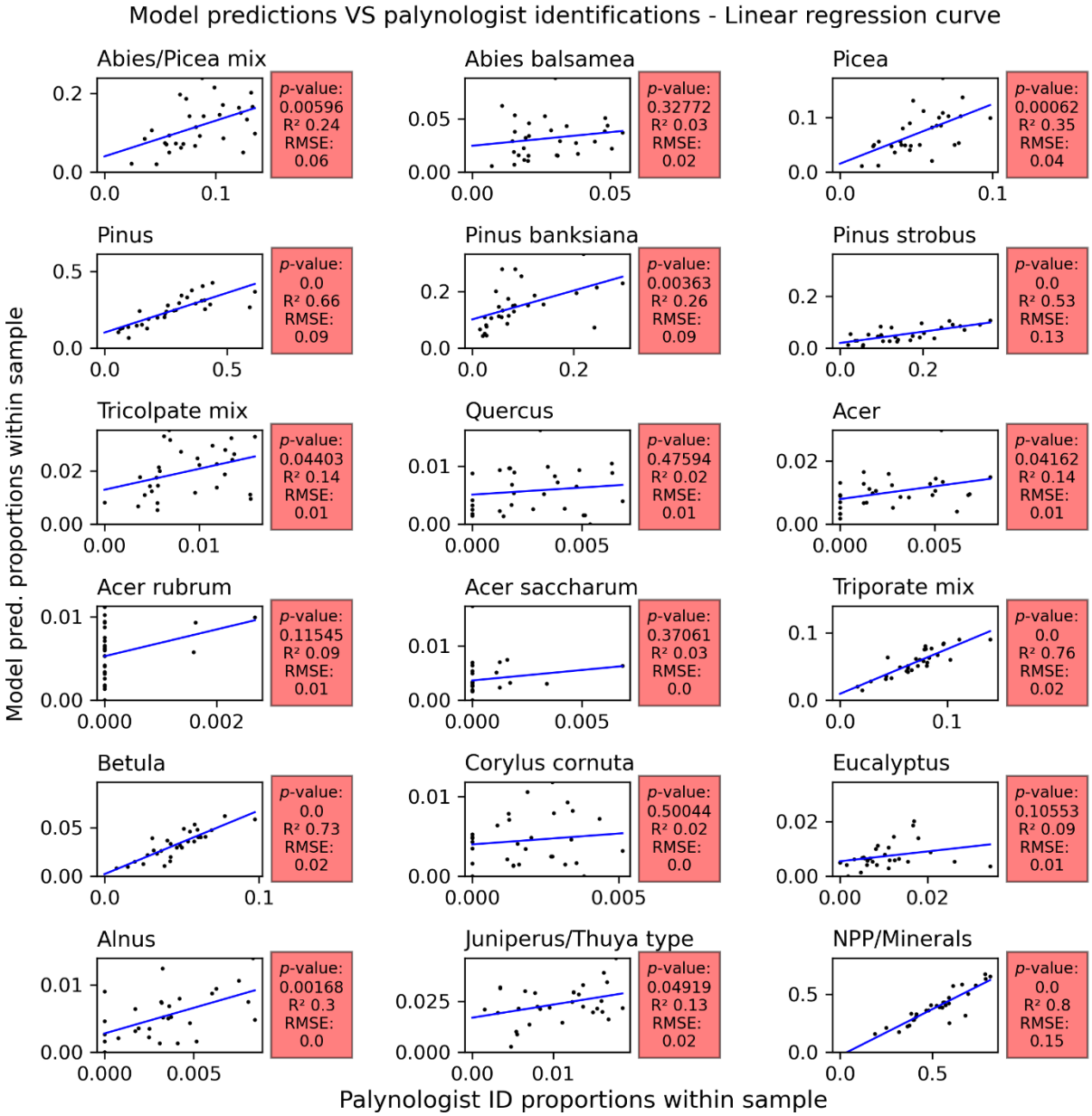

Figure 2-7 - Scatter plot of each possible output class, minus Alnus crispa and rugosa. p-values under 0.05 indicate a correlation according to Student's t-test. The R^2 value indicates the goodness of fit of the regression curve, while the root-mean-square deviation (RMSE) indicates the spread of the data, i.e. *if the goodness of fit is affected by outliers.*

An average of 14.5% of the model's predictions fell under the 0.7 threshold (not shown) and so were classified by the model as *Unknown*. In comparison, 7% of the images were classified as such by the palynologist (not shown). Compared to the CNN test set, this number falls to 4% (Figure

2-2). This indicates that the calibrated model is half as confident as a palynologist when pitted against real world data. When predicting on the non-fossil data, the model is more confident than the palynologist.

Linear regression t-tests have been computed and plotted in order to test for statistical correlation between the two prediction sets. The resulting *P*-values indicate that 12 classes out of 18 show statistical correlation (α =0.05). The classes that failed Student's t-test are Abies (R^2 =0.03; *p*-value=0.33; RMSE=0.02), Quercus (0.02; 0.48; 0.01), both Acer rubrum (0.09; 0.11; 0.01) and saccharum (0.03; 0.37; <0.01), Corylus (0.02; 0.5; <0.01) and Eucalyptus (0.09; 0.11; 0.01). None of these classes were situated at the first level of the classification process. Apart from Abies and Eucalyptus, all the classes that failed Student's t-test have an n<60. A low n also correlates with a low R^2 (*p*-value<0.005). This is a limit inherent to the R-squared metric.

Some palynologist predictions do not fall within the error margin of the model predictions (Figure 2-6). Specifically, plotting the two prediction sets alongside the time axis indicates that predictions tend to differ in older samples. The R-squared results tend to indicate varying regression model performance. Abies predictions show low accuracy, especially in samples older than 6,000 cal. BP, where the model seems to be over predicting. This pattern is also visible in Picea predictions. This coincides with Pinus which shows a pattern of underprediction, particularly in samples 6,000 cal. BP and older.

While Pinus strobus (R^2=0.53; RMSE=0.13) predictions have a relatively high goodness of fit in its linear regression model (Figure 2-7), a pattern of underprediction is clearly visible along the time sequence (Figure 2-6). Although the NPP/minerals class (R^2=0.8; RMSE=0.15) shows only a small tendency towards underprediction, along with Pinus strobus, there are only two classes out of eighteen that display a clear underprediction pattern. It could be inferred that the model is overconfident in its predictions.

Out of all the first-level classes, the Tricolpate (R^2=0.14; RMSE = 0.01) class shows the lowest performance, although it does pass Student's t-test. This is further noticeable in its children classes' performances – Quercus, Acer (R^2 = 0.14; RMSE = 0.01), and Acer rubrum and saccharum.

Both the NPP/minerals and Triporate class (R^2 = 0.76; RMSE = 0.02) show a satisfying performance. Their predicted abundance over time closely follows the traditional palynology results. The Betula class indicates a high goodness of fit (R^2 = 0.73; 0.02) and likewise shows no clear sign of under or over predictions. The Alnus class demonstrates a lower goodness of fit (R^2 = 0.3; RMSE < 0.01) but yet showing signs of correlation to the palynologist predictions (*p*-value = 0.002). However, two of the Triporate child classes, Eucalyptus and Corylus, show low performance. For Eucalyptus, the model predictions differ from the palynologist predictions mainly in the samples situated at the middle of the time sequence (Figure 2-6). The Corylus class errors indicate no time-related patterns. Although a pattern of over-prediction can be observed in the Juniperus/Thuya-type class (R^2 = 0.13; RMSE = 0.02), its predictions roughly follow the variations of the palynologist predictions.

2.4.3 Comparing the fossil test dataset with the full fossil image dataset

The model was used to classify the images of the full fossil image dataset (Figure 2-8). 29,760 images fell under the threshold – an average of 14.4%. On average, 38.5% of each slide's images were classified as an NPP/mineral. A second pollen diagram was plotted, representing 30 samples slides from the lac Bélanger fossil sequence whose pollens have been classified by a palynologist using a light microscope (Figure 2-9) – the traditional method.

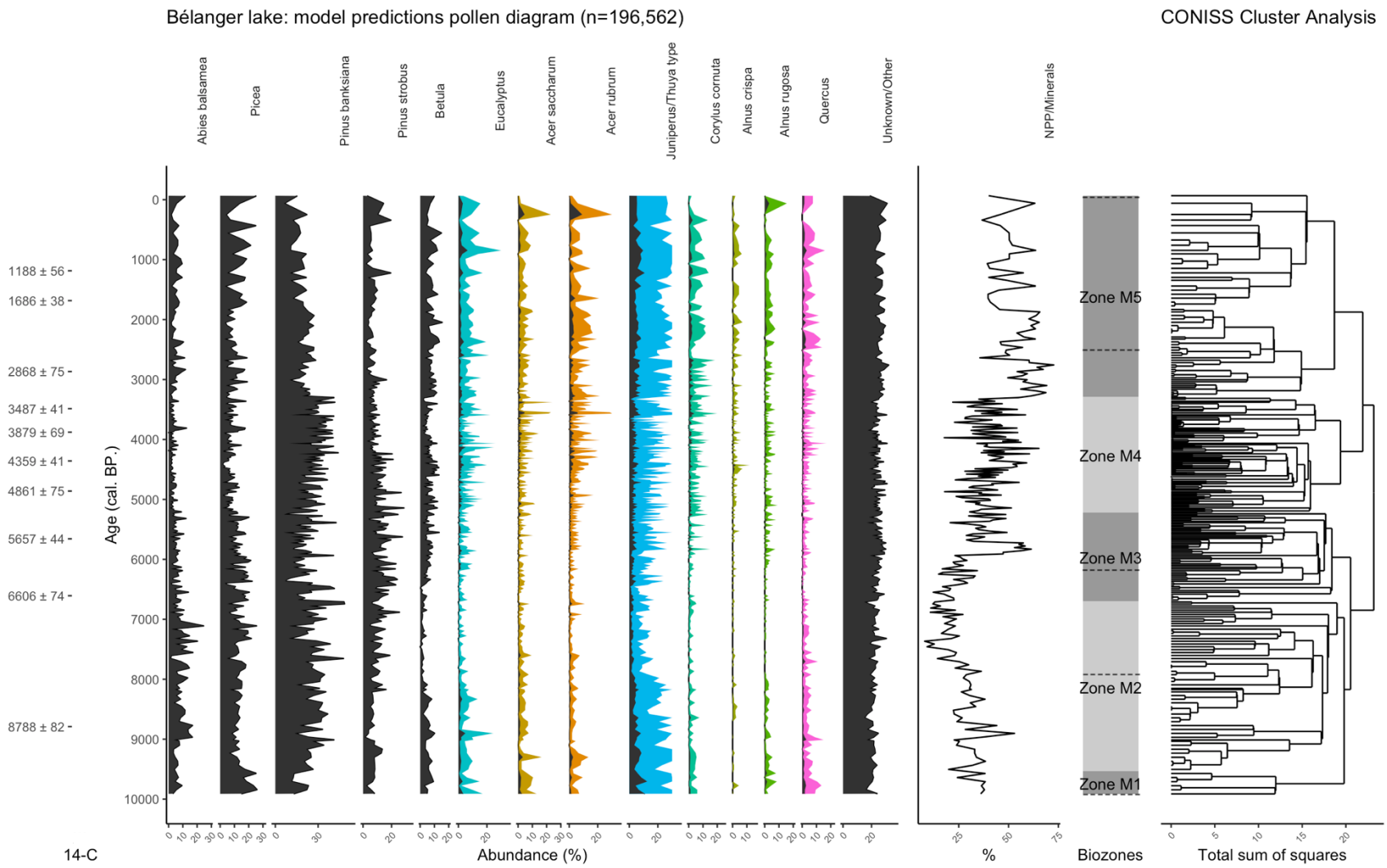

Figure 2-8 : Pollen abundance diagram plotted using the model's predictions on the full fossil dataset, totalling 271 samples. When present, the color fills represent a 5x data exaggeration. The total observed amount of Eucalyptus grains was too low to present the data as pollen influx (pollen/cm²/year), so abundance (%) is used instead. The percentage of NPP/minerals per sample is shown as well as the results of the CONISS cluster analysis and its pollen biozones. The dotted lines cutting across the biozones represent the palynologist biozones (Figure 2-9). The lefthand ticks represent the 14-C dates. See S1 for the age-depth model [Annexe 1].

There are five distinct pollen biozones in Figure 2-8 and four in Figure 2-9. The palynologist diagram's zone P1 (9,900 – 7,950 cal. BP.) suggests early afforestation patterns characterized by high abundances of *J. communis*, *Picea*, *Betula*, *Quercus* and Unknown/Other pollens. The latter two are extra-local influx commonly recorded during periods of low forest density.

On the model's diagram, this period of afforestation is instead split into two disctinct zones. Zone M1 shows the early stages of afforestation characterized by *Quercus* and *Picea* yet fails to register an increase in other unknown extra-local pollens. This further suggests that the model shows overconfidence while identifying pollens belonging to classes it has not been trained on. Zone M2 encloses the later afforestation stage where *P. banksiana* rapidly peaks while *Picea* and *Betula* pollens gradually decrease in abundance. This dynamic is consistent with Figure 2-9.

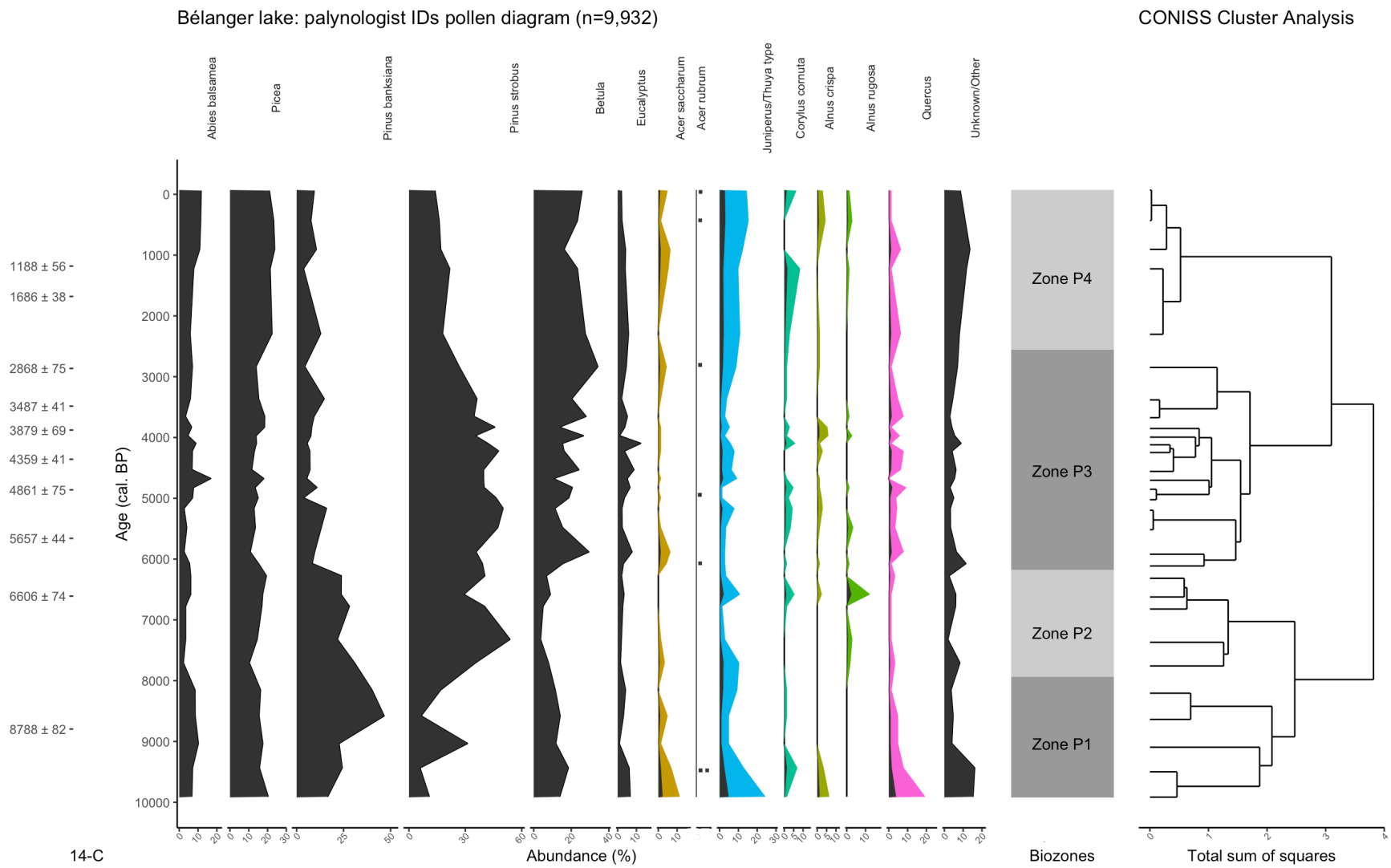

Figure 2-9 : Pollen abundance diagram plotted using data gathered by a palynologist working on a traditional light microscope. When present on the diagrams, the color fills represent a 5x data exaggeration. The results of the CONISS cluster analysis and its resulting biozones are also shown. Considering the low A. rubrum *abundance, its influx is instead represented as dots.*

On the palynologist diagram, the mid-sequence is grouped into two biozones. Zone P2 (7,950 – 6,200 cal. BP.) highlights both *Betula*'s lowest abundance and the gradual replacement of *P. banksiana* by *P. strobus*. Zone P3 (6,200 – 2,550 cal. BP.) is characterized by a progressive drop in *P. strobus* abundance in favour of *Betula.* The mid-sequence also sees a sporadic influx of less abundant species, namely *A. saccharum* and *Alnus.* These general abundance patterns can also be identified on the model's diagram, where the mid-sequence is similarly characterized by a shift from *P. strobus* to *Betula.* However, the 5,000 – 3,000 cal. BP. period showing high *P. banksiana* values is not found on the palynologist diagram. Figure 2-9 conversely shows that most of the *Pinus* influx consists of *P. strobus*. This is consistent with Figure 2-6 which shows that the model tends to overestimate the amount of *P. banksiana* and underestimate the amount of *P. strobus*.

Both diagrams show that the top of the sequence (3,000 cal. BP. onwards) can be grouped in a single zone. Altough the model's last zone begins around 800 years earlier, it is consistent with the palynologist diagram's zone P4. In both zones, the taxa diversity of the influx and the absence of a truly dominant taxon can be interpreted as the stabilization of the local vegetation composition The *Pinus* influx is progressively replaced by other pollens from other coniferous species such as *A. balsamea* and *T. occidentalis*. However, the model fails to register an increase in unknown/other pollens as seen on Figure 2-9.

2.5 Discussion

Our model achieved satisfying results when tested on the test dataset. An APC of 91.2% (with results ranging from 83.3% to 96.6%) is on par with what can be found in the literature. For instance, Bourel et al. (2020) show an APC between 96.3% and 100%, depending on if their model is classifying intact or fossilised pollen. Khanzhina et al.'s model (2018) indicates an APC somewhere between 95.9% and 99.8% while Sevillano et al.'s network (2018) reaches up to 97.9% APC. In Punyasena et al. (2022), the authors train a network on an imbalanced dataset containing 46 different taxa and achieved an 82.3% APC. Their network trained on 25 species scored higher at 89.5% APC.

However, we find that our model does not perform as well on the paleo testing dataset classes. A drop in performance was expected on account of the difference in pollen origin (fresh VS fossil) and their respective extraction methods (section 2.3.2; 2.3.4). The classes showing the poorest correlation are the Tricolpate, Acer saccharum, Corylus and Eucalyptus pollen classes, although their low sample count could be a reason for their poor correlation. Regarding the former, we believe that the inadequate correlation could also be due to an elevated presence of non-*Quercus*, non-*Acer* pollens of either Tricolpate or Tricolporate morphology (*e.g. Fagus* or *Tilia* types) in the paleo testing dataset. Altough such taxa never reached lac Bélanger's latitudes, their combined abundance in similar pollen records can reach up to 4% on account of long-distance dispersal (Bennett, 1985; Fréchette et al., 2018). Since such pollens were not used to train the model, their recurring presence in the Bélanger fossil record might have been enough to throw off the

classification of *Acer* and *Quercus* pollens, thus leading to the over-classification pattern visible in Figure 2-6. Increasing the prediction threshold to 0.9 results in a higher accuracy for both *Acer* and *Quercus* (not shown), further hinting at this conclusion. This would mean that our model could have benefited from being trained on more varied pollen taxa, especially of Tricolpate/Tricolporate morphology.

We find that there is a link between hierarchical level and model performance: the average R^2 is higher (= 0.45) for the CNNs situated at the top of the model (Figure 2-2; CNNs such as Pinus and Triporate) and decreases as the CNNs get deeper (R^2 = 0.25 and 0.06 for the mid and bottom level models, respectively). This suggests that compound errors accumulated over two or three successive classifications could result in a drop in performance in the species-level CNNs situated at the bottom of the model.

Certain species see their correlation decline in samples 6,000 cal. BP. and older, such as *A. balsamea*, *Picea* and *Juniperus/Thuya* type (Figure 2-6). Other species such as *P. banksiana* and *Eucalyptus* register this drop in correlation only throughout the mid-sequence (6,000 – 3,000 cal. BP.). We attribute this temporal differentiation in model correlation seen among classes throughout the sequence to differences in the sediments themselves (*e.g.* diagenetic processes varying through time or periods of higher pollen diversity introducing false positives). This is supported by the fluctuating NPP/minerals values seen in Figure 2-8. The 6,000 – 3,000 cal. BP. period averages 42% NPP/minerals abundance (n=137) while the 9,900 – 6,000 cal. BP. period averages 25% (n=84). An increase in NPP/mineral count signifies an increase in both primary

productivity and diagenetic processes, and consequentially a decrease in image and pollen quality. Such dynamics would be less of an issue were the test images manually cropped from a microscope (Bourel et al., 2020), although this would not be adapted to a large-scale workflow.

Both the Triporate and Betula classes achieved a more than satisfying performance on fossil data. Since pollens of the *Betula* genus are typically found in high abundance across North-Eastern American fossil pollens records (Fréchette et al., 2018), the model's optimal performance in identifying this class was critical. Similarly, the model's performance in classifying fossil *Pinus* genus pollens is satisfactory, although it appears that the different *Pinus* species could at times be confused with one another (Figure 2-6). While diagenetic processes explain part of the problem – especially in mid-Holocene samples – we observe that the slide scanner did not pick up on certain discriminating features present in *Pinus* grains. The protruding distal verruca, usually located inbetween the sacci of *P. strobus* grains, are not visible on Figure 2-3. This could be addressed down the line by using a slide scanner of higher performance.

Nevertheless, numerous classes show both high training accuracy and good performance on the paleo testing dataset. The NPP/minerals class's high classification accuracy assures us that only a minimal amount of non-pollen palynomorphs was mistakenly classified in other classes. Combined with the rapid laboratory treatment method shown in section 2.3.4, the high NPP/minerals classification accuracy indicates that a large-scale fossil pollen classification workflow is indeed possible.

By comparing the pollen biozones in Figure 2-8, we can observe that the variations in the taxa's abundance resemble the ones in the palynologist diagram (Figure 2-9). While the model is certainly overconfident in its predictions, the general patterns in abundance remain constant with the traditional diagram. The very high temporal resolution allows the addition of a fifth pollen zone in the model's diagram, thus illustrating how an increase in temporal resolution can lead to a more precise reconstruction. Moreover, the substantial sample size (196,562 images) used in the reconstruction helps mitigating the model's biases, allowing most taxa's abundance patterns to roughly correlate with the traditional diagram. Both the palynologist and model diagrams show abundance patterns that correspond to what can be found in other reconstructions of Québec's mixed-temperate forest region. These patterns, such as the early *Picea* influx or the 7,500-4,000 cal. BP *P. strobus*-*Betula* dynamic, are observed in regional synthesises such as (Fréchette et al., 2018) and (Richard, 1993). The *Juniperus/Thuya* bimodal distribution also corresponds to what is recorded in mixed-temperate forest pollen diagrams – The early influx is commonly associated with *J. communis*, a boreal species (Fréchette et al., 2018), while the more recent influx corresponds to *T. occidentalis*, an ubiquist species whose steady influx post 5,000 cal. BP rarely dominates pollen assemblages (Richard, 1993). Similarly, the recrudescence of *A. balsamea* in the past 3,000 years is recorded in other mixed-temperate pollen diagrams (Fréchette et al., 2018; Richard, 1993).

2.6 Conclusion

In this paper, we presented a large-scale fossil pollen extraction and classification workflow. We proposed a fossil pollen extraction method that is rapid and that leaves the slides clean enough to scan using an automated microscope. We built upon existing pollen classification models to develop our own model. Our model is trained using fresh pollens and is aimed at classifying pollen grains usually found within North-Eastern American Holocene organic sediment records. Our training accuracy is on par with other models currently found in the literature.

However, when tested against the fossil test dataset, its classification accuracy dropped significantly. This drop in accuracy, attributable to the general quality of the fossil pollens and its resulting images, was an expected setback considering that the model had to be trained on fresh pollens. Still, after classifying a full fossil pollen sequence and comparing the results to traditional palynology, we find that our model picks up on most of the general abundance patterns and variations. Furthermore, its results correspond to other pollen diagrams pertaining to similar environments.

As it currently stands, our model is capable of classifying species present in high abundance but fails to classify pollens of rarer species. Such flaws, combined with the fact that there are some less abundant pollen taxa that are still unknown to our model, indicate that additional work should be spent towards bridging the gap between the training data (fresh pollens) and the target data (fossil pollens). In that sense, online repositories of fossil data could prove useful for training providing that data coherence and uniformity are accounted for. Nevertheless, combined with an

automated slide scanner and our accelerated pollen extraction method, our model serves as a proof of concept for the implementation of a fully automatic large-scale fossil pollen classification workflow.

2.7 Acknowledgements

First, we wish to acknowledge that lac Bélanger is located in Nitaskinan. It is unceded indigenous land that has traditionaly been under the guardianship of the Atikamekw Nehirowisiwok people and upon which they still live to this day. The authors wish to thank A. Hennebelle and L. Peter for sampling the lac in 2017. Special thanks to D. Belamy for technical contributions and to J. Aleman for overall support and guidance in the early stages of the project. We also thank T. Iaculli for proofreading the manuscript and V. Poirier (Ministère des Ressources Naturelles et des Forêts du Québec) for creating the map.

3 Discussion générale

L'objectif de l'article était de créer un modèle de classification entraîné par intelligence-artificielle et capable de classifier des pollens fossiles extraits d'une séquence de sédiments lacustres. Tel que supposé au sein des hypothèses, le modèle subit une perte de performance lors de la classification de pollens fossiles. La diminution de la performance du modèle touche certaines espèces plus que d'autres. En ce sens, trois limites du modèle sont identifiées : i) les espèces plus rares en abondance performent généralement moins bien; c'est le cas des pollens d'*A. saccharum*, dont la présence est surestimée; ii) la performance du modèle varie selon la qualité du sédiment, qui elle-même varie le long de la séquence; iii) certaines espèces sont par moment confondues entre elles. Par exemple, dans la séquence Bélanger, les grains de *P. strobus* et de pins gris (*Pinus banksiana* Lamb.) sont principalement confondus entre 6,000 – 3,000 cal. BP. Toutefois, tel que discuté en détails dans l'article, les difficultés rencontrées par le modèle n'empêchent pas l'identification de patrons généraux (*i.e.* macros) dans les variations en abondance des espèces dans leur ensemble. Il est donc possible de tenter de répondre à la question de recherche de ce mémoire à l'aide des résultats produits par le modèle.

3.1 Nouvelles données et interprétation des dynamiques holocènes

L'analyse des charbons fossiles a permis de reconstruire l'histoire des feux du lac Bélanger. Elle a été conduite à un pas centimétrique (*e.g.* sur tous les niveaux de la carotte). Un traitement à l'hydrochlorite de sodium effectué sur 1 cm^3 de chaque échantillon suivi d'un tamisage à 150 µm a permis d'isoler chaque macrocharbons. À l'aide du logiciel de microscopie Winseedle, le nombre et la surface totale des charbons de bois de chaque niveau de la carotte a été enregistré. En se servant de la surface totale de charbon par échantillon (μm^2), l'histoire des feux a été reconstruite

grâce à la librairie *Tapas* (Finsinger et Bonnici, 2022), elle-même basée sur les travaux de Higuera (2009). L'utilisation de la librairie *Tapas*, privilégiée grâce à son intégration au langage R, reconstruit l'histoire des feux en incorporant le modèle âge/profondeur (Annexe 1). Ceci permet d'obtenir le taux d'accumulation de charbon (Char Acc, $mm^{-2} \cdot cm^{-2} \cdot année^{-1}$). Ce taux d'accumulation est ensuite comparé à un taux d'accumulation d'arrière-plan (bruit, charbons d'origine extra-locale ou charbons locaux ne se sédimentant que plusieurs années après le feu), identifiant de ce fait les événements de feux lorsque le taux d'accumulation d'arrière-plan est surpassé.

La Figure 3-1 représente le diagramme pollinique généré à l'aide des prédictions du modèle auquel a été rajouté l'histoire des feux. La Figure 3-2, représentant les courbes de fréquence des feux et d'accumulation de charbon auxquelles a été rajoutée la courbe d'abondance des pollens d'*A. saccharum*, indique que l'histoire des feux peut être divisée en quatre périodes. Ces périodes concordent grossièrement aux zones d'accumulation pollinique telles que décrites dans l'article (*pollen zones*).

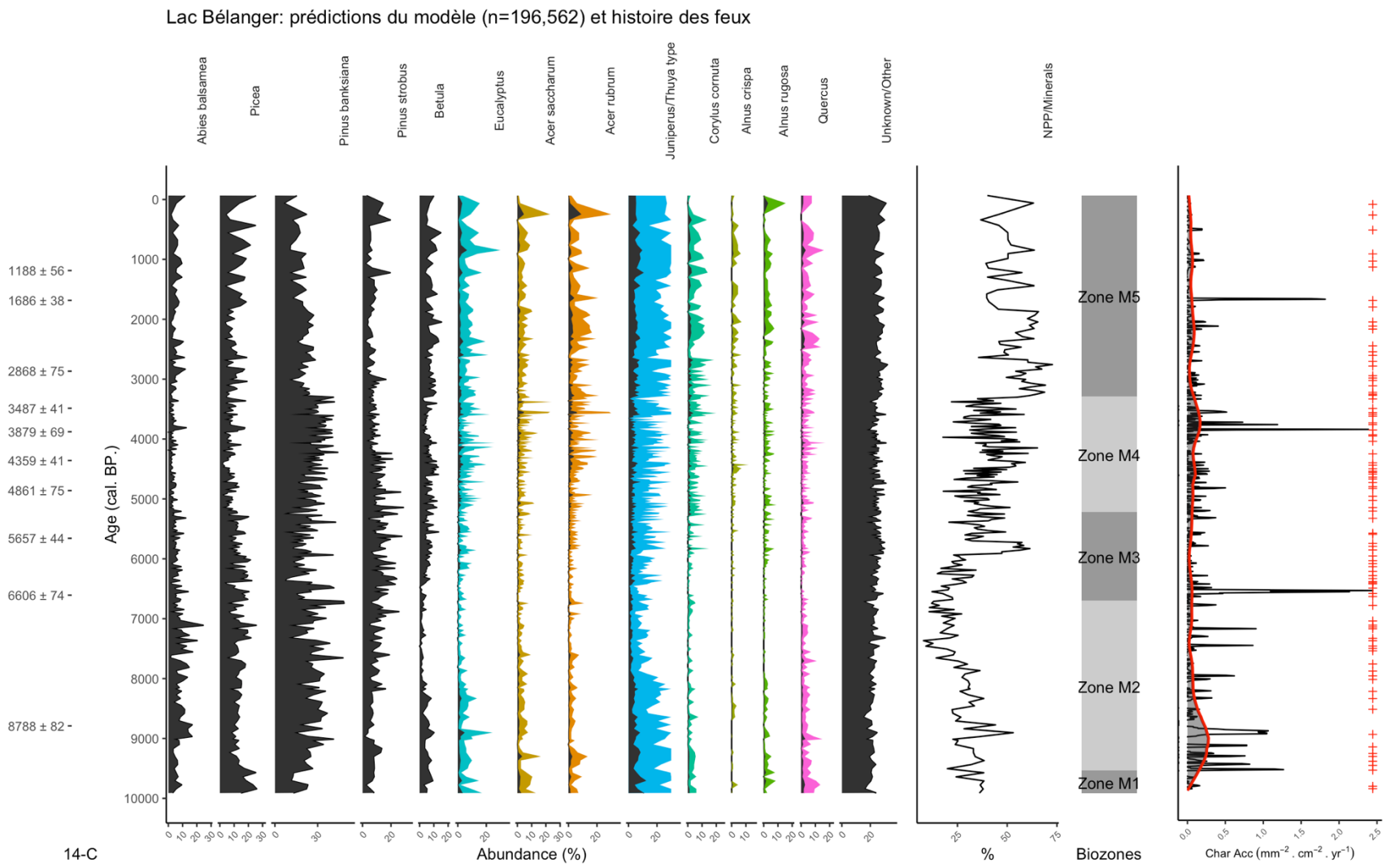

Figure 3-1: Diagramme pollinique du lac Bélanger et histoire des feux. La reconstruction de la végétation a été complétée à l'aide du modèle. L'histoire des feux a été reconstruite au travers l'analyse des charbons fossiles. Les croix rouges représentent l'histoire des feux, tandis que la courbe rouge représente le seuil d'accumulation régionale (bruit). Un événement de feu est identifié lorsque l'accumulation surpasse le seuil. L'accumulation sous le seuil représente des feux distants, ou bien un délai dans la déposition de charbons d'un feu précédant.

Les zones M1 et M2 (9,990 – 6,800 cal. BP) sont caractérisées par un régime de feux fréquents. Les pics d'accumulation franchissent nettement le seuil d'influx régional et coïncident avec les périodes les plus chaudes de l'OCH. Une certaine accalmie du régime de feu, autour de 8,000 cal. BP, précède toutefois une augmentation de la fréquence des feux culminant dans la zone M3. La végétation qui succède habituellement le passage des glaciers étant composée d'espèces boréales formant des forêts ouvertes (*e.g. A. balsamea*, *P. banksiana*, *Picea*, *J. Communis*, *Alnus*) (Blarquez et Aleman, 2016; Fréchette et al., 2018; Richard, 1993), le signal pollinique d'*A. saccharum* représente du transport de longue distance venu du sud. Dès 8,500 cal. BP, *P. banksiana* perd en abondance face à *P. strobus*.

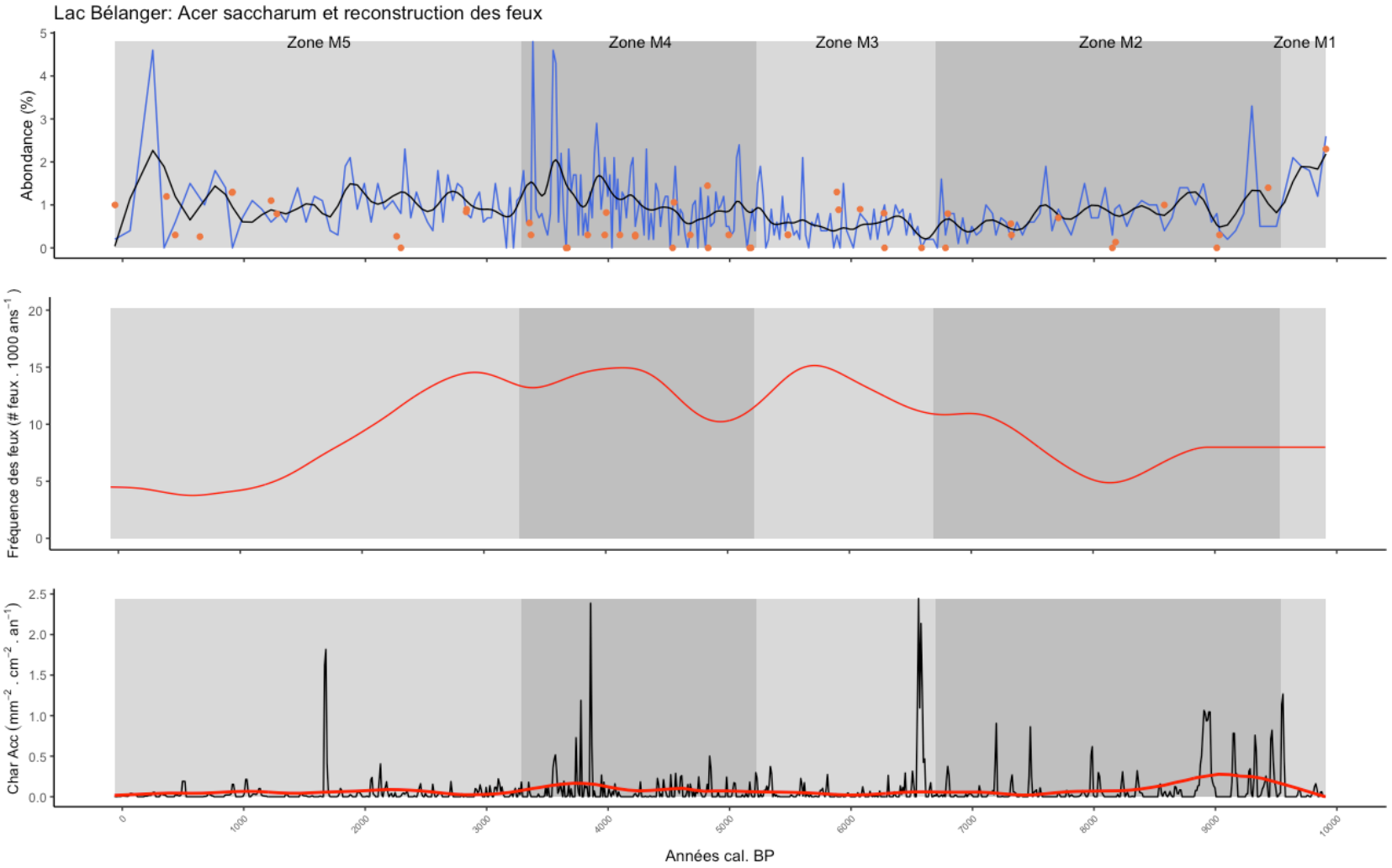

*Figure 3-2 : Reconstruction d'*A. saccharum, *fréquence des feux et accumulation des charbons fossiles. Le graphique du haut représente l'abondance en pollen* d'A. saccharum *le long de la séquence. La courbe bleue est l'abondance telle que prédite par le modèle. La courbe noire sur le même graphique indique un* smoothing *(0.35) de l'abondance. Les points oranges (n=50) représentent l'abondance d'*A. saccharum *observée par la palynologie traditionnelle. Le graphique du milieu représente la fréquence des feux (feux/1,000 ans;* smooth *0.45). Le graphique du bas représente l'accumulation de charbon en fonction du temps, tel que décrite à la Figure 3-1.*

Il est alors possible de constater les débuts de la dynamique de *P. strobus/Betula* observée dans l'article, dans d'autres reconstructions en forêt mixte (Fréchette et al., 2018; Larochelle et al., 2018; Richard, 1993) ainsi que sur les érablières de Paillard (2018) (Figure 1-1). La forte abondance du genre *Pinus* durant cette période coïncide avec l'absence des espèces décidues (*Betula, Acer*) dans le diagramme pollinique. Considérant à la fois le biais du modèle, qui favorise le *P. banksiana* face à *P. strobus*, ainsi que les dynamiques de *Pinus* près des sites du lac Lili (Bajolle, 2018), Chasseur (Paillard, 2018), et de la tourbière Parent (Larochelle et al., 2018), il est possible d'inférer la présence d'une forêt conifférienne dominée par *P. strobus* au lac Bélanger dès 8,000 cal. BP qui culmine en 5,000 cal. BP. Conséquemment, considérant les propriétés de l'espèce, la présence de *P. strobus* suggère des feux de basse sévérité (Engelmark et al., 2000) bien que fréquents (Figure 3-2).

La zone M3 (6,800 – 5,200 cal. BP) se distingue par l'intensification de la fréquence des feux qui s'effectue de façon synchrone à l'arrivée de *Betula* dans le paysage ainsi qu'à la raréfaction d'*A. balsamea* et de *Picea* (Figure 3-1). Le signal d'*A. saccharum*, faible mais constant (Figure 3-2), n'indique pas une présence locale de l'espèce.

La zone M4 (5,200 – 3,200 cal. BP) est marquée par le climat plus froid du néoglaciaire, lui-même accompagné d'une nouvelle augmentation de la fréquence des feux. Alors qu'une baisse généralisée de la biomasse est constatée chez Blarquez et Aleman (2016), *P. strobus* se fait plus rare au sein de la sapinière à bouleau blanc (Bajolle, 2018; Larochelle et al., 2018; Paillard, 2018) et des environs du lac Bélanger en réponse à ces feux. Au nord, dans le domaine de la sapinière à bouleau blanc, *B. alleghaniensis*, moins adapté aux feux que *B. papyrifera*, coexiste encore avec ce dernier (Larochelle et al., 2018). Plus au sud, dans le domaine de la sapinière à bouleau jaune, la présence locale de *B. alleghaniensis* au lac Bélanger et la stabilité de son influx (*i.e.* l'absence

de perturbations causant l'exclusion de l'espèce), indiquent la possibilité que les changements dans le régime de feu ne se soient pas traduits par une sévérité accrue près du site à l'étude. Les prédictions du modèle, qui recensent une forte hausse de l'abondance du pollen d'*A. saccharum* durant cette période, suggèrent un établissement au moins régional de l'espèce en 4,800 cal. BP (Figure 3-2). En atténuant les effets prioritaires entretenus par les espèces coniférienes (Solarik et al., 2020) ainsi qu'en diminuant les effets de l'herbivorie et des intempéries (Evans et al., 2020), ce processus migratoire aurait pu être facilité par la présence de *Betula* à l'échelle du peuplement. Cet établissement régional correspond à l'établissement des érablières du lac Fur dans le sud-ouest (7,800 – 5,100 cal. BP) et du lac Chasseur à l'ouest (5,550 – 4,400 cal. BP) (Paillard, 2018). Il concorde avec un signal régional de l'espèce dans les reconstructions des lacs Bride (*circa* 7,000 cal. BP; Richard, 1993), Louis (5,500 cal. BP; Fréchette et al., 2018; Vincent, 1973), Martini (*circa* 4,000 cal. BP; Richard, 1993) et Francis (3,600 cal. BP; Carcaillet et al., 2001). Bien que le régime de perturbation et la présence de peuplements majoritairement décidus aurait pu permettre l'établissement local d'Acer *saccharum* au lac Bélanger, l'absence d'un signal pollinique suffisant et continu obtenu par palynologie traditionnelle empêche d'attester de sa présence locale (Figure 3-2). Conséquemment, la présence locale de l'espèce et son maintien subséquent ne peuvent être datés qu'à partir de 1,200 cal. BP, quoiqu'il soit probable que l'espèce s'y soit installée avant. Un décomptage plus exhaustif des pollens d'*Acer saccharum*, tel qu'entrepris lors de l'étude de Paillard (2018), pourrait permettre de corroborer les reconstructions du modèle. Il s'agit d'une méthode plus adaptée lorsqu'il est question de reconstruire les dynamiques d'une espèce au pollen rare (Birks et Birks, 1980).

4 Conclusion

L'objectif premier de ce mémoire de recherche, outre la création du modèle vu dans l'article, était de déterminer quand et sous quelles conditions *A. saccharum* s'est installé aux abords du lac Bélanger. À cet effet, les données polliniques suggèrent une présence régionale de l'espèce en 4,800 cal. BP et un établissement local en 1,200 cal. BP. Ces résultats écartent la possibilité d'un établissement datant de l'Optimum climatique Holocène. L'absence d'une migration nordique de l'espèce durant les périodes plus chaudes de l'OCH démontre que la répartition d'*A. saccharum* n'est pas uniquement contrôlée par le climat, mais plutôt par i) la sévérité du régime de perturbation et ii) la présence d'espèces décidues facilitant sa transition (*Betula*) (Collin et al., 2018; Evans et al., 2020; Solarik, 2017).

Les dynamiques holocènes d'*A. saccharum* en situation marginale nordique illustrent la complexité de l'espèce et de son écologie. Face à un réchauffement global forçant les espèces tempérées à migrer au-delà de leur limite nord de répartition (Chen et al., 2011), les résultats de ce projet de maîtrise soulignent la nécessité de protéger les populations nordiques d'érable à sucre, sachant qu'elles pourront faciliter les migrations provenant de l'aire de répartition continue.

Le modèle créé durant le projet – le premier du genre – est une preuve de concept réussie. Son utilisation, combinée au processus de travail (*workflow*) proposé dans l'article, a permis l'obtention d'une reconstruction de l'histoire de la végétation à la fois facilement reproductible et pouvant être comparée à la palynologie traditionnelle. L'analyse de haute résolution temporelle offerte par la palynologie automatique permet une précision accrue lors des reconstructions paléo-environnementales et rendra possible l'identification de patrons écosystémiques fins. Une continuation des travaux est nécessaire en vue de tracer un pont entre l'analyse à échelle temporelle

longue (migratoire, voire évolutive) et à échelle temporelle courte (dynamiques ponctuelles inhérentes aux sites et comportements post-perturbations). L'incertitude des interprétations paléo-environnementales causée par le biais d'entraînement des modèles est le frein principal à l'automatisation de la paléo-palynologie. En ce sens, la réduction du biais des modèles de classification devrait être vue comme étant la prochaine étape à suivre.

5 Références

Ali, A., Asselin, H., Larouche, A. C., Bergeron, Y., Carcaillet, C. et Richard, P. J. H. (2008). Changes in fire regime explain the Holocene rise and fall of Abies balsamea in the coniferous forests of western Québec, Canada. *The Holocene*, *18*(5), 693-703. https://doi.org/10.1177/0959683608091780

Ali, A., Blarquez, O., Girardin, M. P., Hely, C., Tinquaut, F., El Guellab, A., Valsecchi, V., Terrier, A., Bremond, L., Genries, A., Gauthier, S. et Bergeron, Y. (2012). Control of the multimillennial wildfire size in boreal North America by spring climatic conditions. *Proceedings of the National Academy of Sciences*, *109*(51), 20966-20970. https://doi.org/10.1073/pnas.1203467109

Ali, A., Carcaillet, C. et Bergeron, Y. (2009). Long-term fire frequency variability in the eastern Canadian boreal forest: the influences of climate vs. local factors. *Global Change Biology*, *15*(5), 1230-1241. https://doi.org/10.1111/j.1365-2486.2009.01842.x

Alzubaidi, L., Zhang, J., Humaidi, A. J., Al-Dujaili, A., Duan, Y., Al-Shamma, O., Santamaría, J., Fadhel, M. A., Al-Amidie, M. et Farhan, L. (2021). Review of deep learning: concepts, CNN architectures, challenges, applications, future directions. *Journal of Big Data*, *8*(1), 53. https://doi.org/10.1186/s40537-021-00444-8

Bajolle, L. (2018). *Reconstitution des paléotempératures holocènes de la forêt boréale conifèrienne de l'ouest du Québec basée sur une approche multi-indicateurs* [doctorat, Université Montpellier]. https://theses.hal.science/tel-01908668

Bajolle, L., Larocque-Tobler, I., Gandouin, E., Lavoie, M., Bergeron, Y. et Ali, A. A. (2018). Major postglacial summer temperature changes in the central coniferous boreal forest of

Quebec (Canada) inferred using chironomid assemblages. *Journal of Quaternary Science*, *33*(4), 409-420. https://doi.org/10.1002/jqs.3022

Bennett, K. D. (1985). The Spread of Fagus grandifolia Across Eastern North America During the Last 18 000 years. *Journal of Biogeography*, *12*(2), 147. https://doi.org/10.2307/2844838

Bennett, K. D. (1996). Determination of the number of zones in a biostratigraphical sequence. *New Phytologist*, *132*(1), 155-170. https://doi.org/10.1111/j.1469-8137.1996.tb04521.x

Bergeron, Y., Gauthier, S., Flannigan, M. et Kafka, V. (2004). Fire regimes at the transition between mixedwood and coniferous boreal forest in Northwestern Quebec. *Ecology*, *85*(7), 1916-1932. https://doi.org/10.1890/02-0716

Birks, H. et Birks, H. (1980). Principles and methods of pollen analysis. Dans *Quaternary Palaeoecology* (Illustrated, p. 157-176). University Park Press.

Blarquez, O. et Aleman, J. C. (2016). Tree biomass reconstruction shows no lag in postglacial afforestation of eastern Canada. *Canadian Journal of Forest Research*, *46*(4), 485-498. https://doi.org/10.1139/cjfr-2015-0201

Bourel, B., Marchant, R., de Garidel-Thoron, T., Tetard, M., Barboni, D., Gally, Y. et Beaufort, L. (2020). Automated recognition by multiple convolutional neural networks of modern, fossil, intact and damaged pollen grains. *Computers & Geosciences*, *140*, 104498. https://doi.org/10.1016/j.cageo.2020.104498

Brisson, J., Bergeron, Y. et Bouchard, A. (1988). Les successions secondaires sur sites mésiques dans le Haut-Saint-Laurent, Québec, Canada. *Canadian Journal of Botany*, *66*(6), 1192-1203. https://doi.org/10.1139/b88-170

Campbell, J. F. E., Fletcher, W. J., Hughes, P. D. et Shuttleworth, E. L. (2016). A comparison of pollen extraction methods confirms dense-media separation as a reliable method of pollen preparation: Dense-media separation as a reliable method of pollen preparation. *Journal of Quaternary Science*, *31*(6), 631-640. https://doi.org/10.1002/jqs.2886

Carcaillet, C., Bergeron, Y., Richard, P. J. H., Fréchette, B., Gauthier, S. et Prairie, Y. T. (2001). Change of fire frequency in the eastern Canadian boreal forests during the Holocene: does vegetation composition or climate trigger the fire regime?: *Holocene fire frequency changes in Canadian boreal forests*. *Journal of Ecology*, *89*(6), 930-946. https://doi.org/10.1111/j.1365-2745.2001.00614.x

Carcaillet, C., Richard, P. J. H., Bergeron, Y., Fréchette, B. et Ali, A. A. (2010). Resilience of the boreal forest in response to Holocene fire-frequency changes assessed by pollen diversity and population dynamics. *International Journal of Wildland Fire*, *19*(8), 1026. https://doi.org/10.1071/WF09097

Chen, I.-C., Hill, J. K., Ohlemuller, R., Roy, D. B. et Thomas, C. D. (2011). Rapid Range Shifts of Species Associated with High Levels of Climate Warming. *Science*, *333*(6045), 1024-1026. https://doi.org/10.1126/science.1206432

Collin, A., Messier, C., Kembel, S. W. et Bélanger, N. (2018). Can sugar maple establish into the boreal forest? Insights from seedlings under various canopies in southern Quebec. *Ecosphere*, *9*(1). https://doi.org/10.1002/ecs2.2022

Cyr, D., Gauthier, S. et Bergeron, Y. (2007). Scale-dependent determinants of heterogeneity in fire frequency in a coniferous boreal forest of eastern Canada. *Landscape Ecology*, *22*(9), 1325-1339. https://doi.org/10.1007/s10980-007-9109-3

Daood, Riberio, et Bush. (2018, 10 mai). *Sequential recognition of pollen grain Z-stacks by combining CNN and RNN*. The Thirty-First International Florida Artificial Intelligence Research Society Conference, Melboure, Floride, US (p. 8-13).

Dunker, S., Motivans, E., Rakosy, D., Boho, D., Mäder, P., Hornick, T. et Knight, T. M. (2020). Pollen analysis using multispectral imaging flow cytometry and deep learning. *New Phytologist*, nph.16882. https://doi.org/10.1111/nph.16882

Engelmark, O., Bergeron, Y. et Flannigan, M. D. (2000). Age Structure of Eastern White Pine, Pinus strobus L., at its Northern Distribution Limit in Quebec. *The Canadian Field-Naturalist*, *114*(4), 601-604.

Evans, P., Crofts, A. L. et Brown, C. D. (2020). Biotic filtering of northern temperate tree seedling emergence in beyond-range field experiments. *Ecosphere*, *11*(5). https://doi.org/10.1002/ecs2.3108

Fægri, K., Iversen, J., Kaland, P. E. et Krzywinski, K. (2007). *Textbook of pollen analysis* (IV ed). Blackburn Press.

Finsinger, W. et Bonnici, I. (2022, 10 mars). tapas: an R package to perform trend and peaks analysis. Zenodo. https://doi.org/10.5281/ZENODO.6344463

Fréchette, B., Richard, P. J. H., Grondin, P., Lavoie, M. et Larouche, A. C. (2018). *Histoire postglaciaire de la végétation et du climat des pessières et des sapinières de l'ouest du Québec*. Gouvernement du Québec, ministère des Forêts, de la Faune et des Parcs, Direction de la recherche forestière.

Geus, A. R. de, Barcelos, C. A. Z., Batista, M. A. et Silva, S. F. da. (2019, septembre). *Large-scale Pollen Recognition with Deep Learning*. 2019 27th European Signal Processing

Conference (EUSIPCO), A Coruna, Spain (p. 1-5). https://doi.org/10.23919/EUSIPCO.2019.8902735

Guo, C., Pleiss, G., Sun, Y. et Weinberger, K. Q. (2017). On Calibration of Modern Neural Networks. https://doi.org/10.48550/ARXIV.1706.04599

Higuera. (2009). CharAnalysis: Diagnostic and analytical tools for sediment-charcoal analysis. https://github.com/phiguera/CharAnalysis

Holt, K., Allen, G., Hodgson, R., Marsland, S. et Flenley, J. (2011). Progress towards an automated trainable pollen location and classifier system for use in the palynology laboratory. *Review of Palaeobotany and Palynology*, *167*(3-4), 175-183. https://doi.org/10.1016/j.revpalbo.2011.08.006

Holt, K. et Bennett, K. D. (2014). Principles and methods for automated palynology. *New Phytologist*, *203*(3), 735-742. https://doi.org/10.1111/nph.12848

Kaya, Y., Pınar, S. M., Erez, M. E. et Fidan, M. (2013). An expert classification system of pollen of Onopordum using a rough set approach. *Review of Palaeobotany and Palynology*, *189*, 50-56. https://doi.org/10.1016/j.revpalbo.2012.11.004

Khanzhina, N., Putin, E., Filchenkov, A. et Zamyatina, E. (2018). Pollen Grain Recognition Using Convolutional Neural Network. *Computational Intelligence*, 6.

Lagerstrom, R., Arzhaeva, Y., Bischof, L., Haberle, S., Hopf, F. et Lovell, D. (2013). *A comparison of classification algorithms within the Classifynder pollen imaging system*. 2013 INTERNATIONAL SYMPOSIUM ON COMPUTATIONAL MODELS FOR LIFE SCIENCES, Sydney, Australia (p. 250-259). https://doi.org/10.1063/1.4825017

Larochelle, É., Lavoie, M., Grondin, P. et Couillard, P.-L. (2018). Vegetation and climate history of Quebec's mixed boreal forest suggests greater abundance of temperate species during

the early- and mid-Holocene. *Botany*, *96*(7), 437-448. https://doi.org/10.1139/cjb-2017-0182

Louveaux, J., Maurizio, A. et Vorwohl, G. (1978). Methods of Melissopalynology. *Bee World*, *59*(4), 139-157. https://doi.org/10.1080/0005772X.1978.11097714

MacLeod, N., Benfield, M. et Culverhouse, P. (2010). Time to automate identification. *Nature*, *467*(7312), 154-155. https://doi.org/10.1038/467154a

Mander, L., Baker, S. J., Belcher, C. M., Haselhorst, D. S., Rodriguez, J., Thorn, J. L., Tiwari, S., Urrego, D. H., Wesseln, C. J. et Punyasena, S. W. (2014). Accuracy and consistency of grass pollen identification by human analysts using electron micrographs of surface ornamentation. *Applications in Plant Sciences*, *2*(8), 1400031. https://doi.org/10.3732/apps.1400031

Nakagawa, T., Brugiapaglia, E., Digerfeldt, G., Reille, M., Beaulieu, J.-L. D. et Yasuda, Y. (2008). Dense-media separation as a more efficient pollen extraction method for use with organic sediment/deposit samples: comparison with the conventional method. *Boreas*, *27*(1), 15-24. https://doi.org/10.1111/j.1502-3885.1998.tb00864.x

Nguyen, N. R., Donalson-Matasci, M. et Shin, M. C. (2013, janvier). *Improving pollen classification with less training effort*. 2013 IEEE Workshop on Applications of Computer Vision (WACV), Clearwater Beach, FL, USA (p. 421-426). https://doi.org/10.1109/WACV.2013.6475049

Nolet, P., Delagrange, S., Bouffard, D., Doyon, F. et Forget, E. (2008). The successional status of sugar maple (Acer saccharum), revisited. *Annals of Forest Science*, *65*(2), 208-208. https://doi.org/10.1051/forest:2007091

O'Keefe, J. M. K. et Wymer, C. L. (2017). An alternative to acetolysis: application of an enzyme-based method for the palynological preparation of fresh pollen, honey samples and bee capsules. *Palynology*, *41*(1), 117-120. https://doi.org/10.1080/01916122.2015.1103321

Paillard, J. (2018). *Dynamique Holocène de l'érable à sucre (Acer saccharum Marsh) dans l'ouest du Québec* [mémoire, Université du Québec à Montréal]. https://archipel.uqam.ca/11982/1/M15782.pdf

Payette, S., Frégeau, M., Couillard, P.-L., Pilon, V. et Laflamme, J. (2018). Sugar maple (*Acer saccharum*) at its northeastern range limit: a fire-resilient tree species. *Botany*, *96*(6), 411-423. https://doi.org/10.1139/cjb-2018-0016

Pedersen, B., Bailey, D. G., Hodgson, R. M., Holt, K. et Marsland, S. (2017, décembre). *Model and feature selection for the classification of dark field pollen images using the classifynder system*. 2017 International Conference on Image and Vision Computing New Zealand (IVCNZ), Christchurch, New Zealand (p. 1-5). https://doi.org/10.1109/IVCNZ.2017.8402498

Pilon, V. et Payette, S. (2015). Sugar maple (*Acer saccharum*) forests at their northern distribution limit are recurrently impacted by fire. *Canadian Journal of Forest Research*, *45*(4), 452-462. https://doi.org/10.1139/cjfr-2014-0322

Pitelka, L. (1997). Plant Migration and Climate Change. *American Scientist*, *85*, 464-473.

Punyasena, S. W., Haselhorst, D. S., Kong, S., Fowlkes, C. C. et Moreno, J. E. (2022). Automated identification of diverse Neotropical pollen samples using convolutional neural networks. *Methods in Ecology and Evolution*, *13*(9), 2049-2064. https://doi.org/10.1111/2041-210X.13917

Richard, P. J. H. (1993). Origine et dynamique postglaciaire de la forêt mixte au Québec. *Review of Palaeobotany and Palynology*, *79*(1-2), 31-68. https://doi.org/10.1016/0034-6667(93)90037-U

Richard, P. J. H. (1995). Le couvert végétal du Québec-Labrador il y a 6000 ans BP : essai, *49*(1), 25. https://doi.org/10.7202/033033ar

Saucier, J.-P., Grondin, P., Robitaille, A. et Gosselin, J. (2009). Chapitre 4: Écologie forestière. Dans Ordre des ingénieurs forestiers du Québec (dir.), *Manuel de foresterie* (2e éd., p. 167-315). Éditions MultiMondes.

Sevillano, V. et Aznarte, J. L. (2018). Improving classification of pollen grain images of the POLEN23E dataset through three different applications of deep learning convolutional neural networks. *PLOS ONE*, *13*(9), e0201807. https://doi.org/10.1371/journal.pone.0201807

Sevillano, V., Holt, K. et Aznarte, J. L. (2020). Precise automatic classification of 46 different pollen types with convolutional neural networks. *PLOS ONE*, *15*(6), e0229751. https://doi.org/10.1371/journal.pone.0229751

Simonyan, K. et Zisserman, A. (2015, 10 avril). Very Deep Convolutional Networks for Large-Scale Image Recognition. arXiv. http://arxiv.org/abs/1409.1556

Solarik, K. (2017). *Limited Migration: Will Sugar Maple Tap Out to Climate Change* [doctorat, Université du Québec à Montréal]. http://www.kevinsolarik.com/wp-content/uploads/2015/12/solarik-phd-thesis.pdf

Solarik, K., Cazelles, K., Messier, C., Bergeron, Y. et Gravel, D. (2020). Priority effects will impede range shifts of temperate tree species into the boreal forest. *Journal of Ecology*, *108*(3), 1155-1173. https://doi.org/10.1111/1365-2745.13311

Suanno, C., Aloisi, I., Fernández-González, D. et Del Duca, S. (2021). Pollen forecasting and its relevance in pollen allergen avoidance. *Environmental Research*, *200*, 111150. https://doi.org/10.1016/j.envres.2021.111150

Terasmae, J. et Anderson, T. W. (1970). Hypsithermal range extension of white pine (*Pinus strobus* L.) in Quebec, Canada. *Canadian Journal of Earth Sciences*, *7*(2), 406-413. https://doi.org/10.1139/e70-035

Vincent, J. S. (1973). A palynological study for the little clay belt, northwestern Québec. *Le Naturaliste canadien*, *100*, 59-70.

Wotton, B. M., Nock, C. A. et Flannigan, M. D. (2010). Forest fire occurrence and climate change in Canada. *International Journal of Wildland Fire*, *19*(3), 253. https://doi.org/10.1071/WF09002

6 Annexes

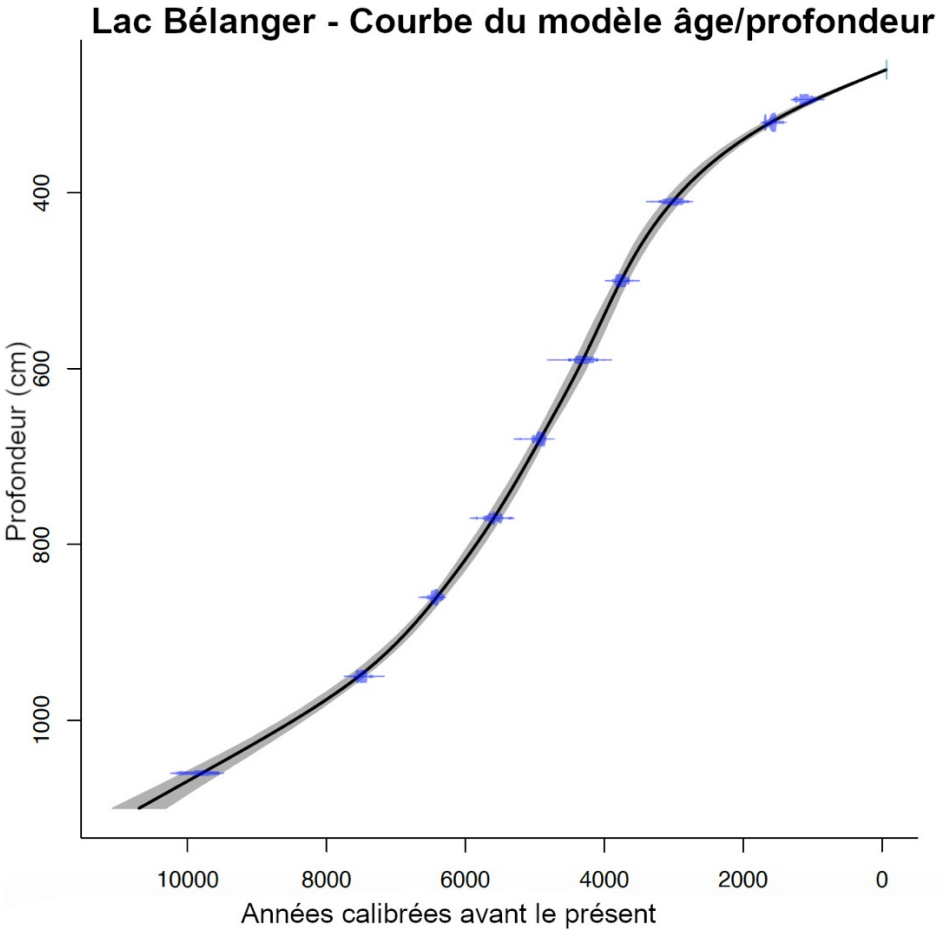

Annexe 1 – Courbe tracée par le modèle âge/profondeur. Calibrée à l'aide de la courbe OxCal v4.3. Données rabattues par lissage *Smooth Spline.* Le remplissage gris représente l'intervalle de confiance des dates interpolées ($\alpha = 0.05$); le remplissage bleu représente l'intervalle de confiance des dates radiocarbone ($\alpha = 0.05$).

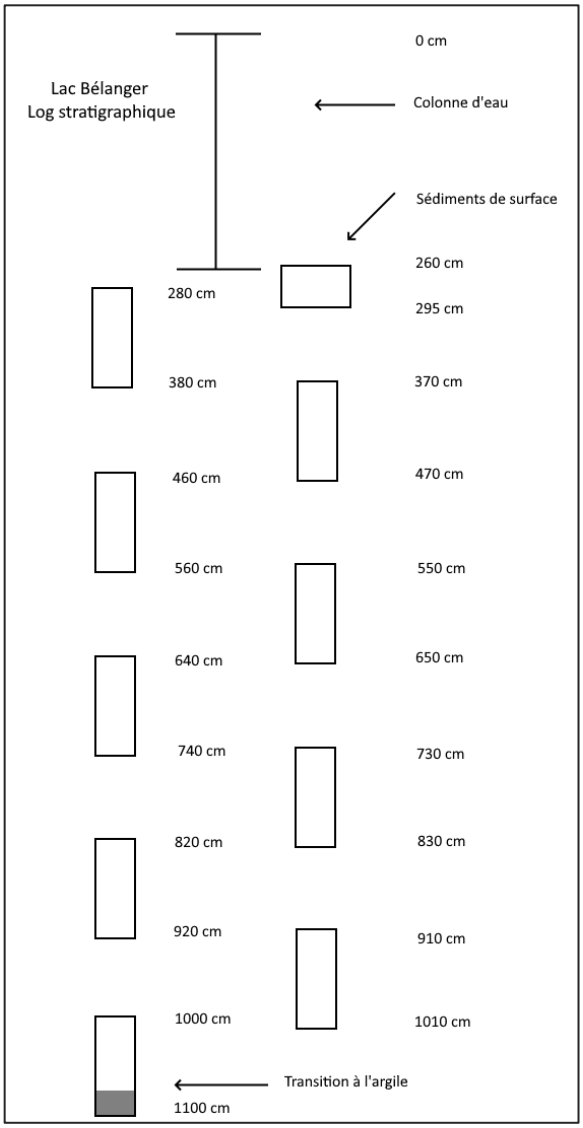

Annexe 2 – Schéma des sédiments du lac Bélanger

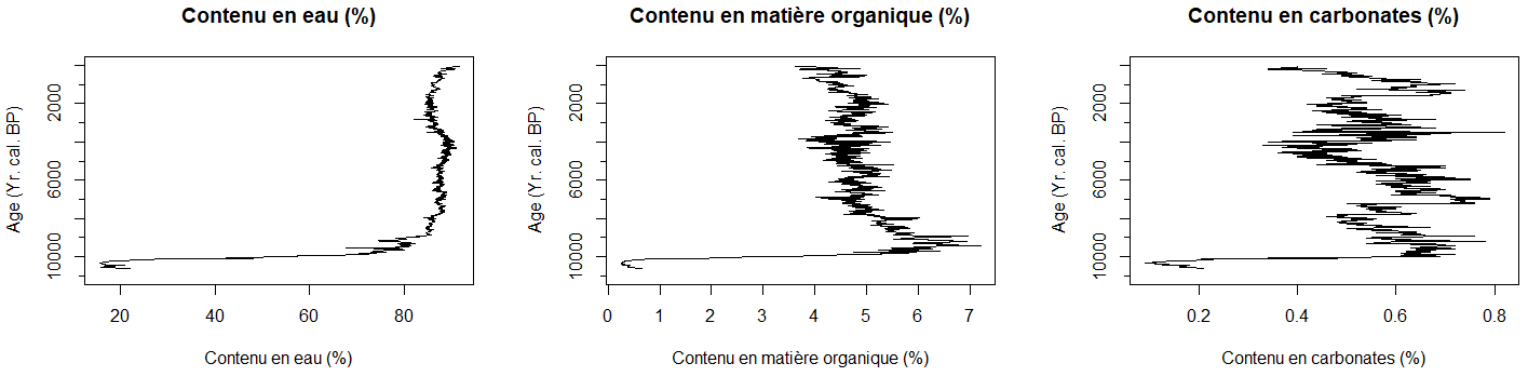

Annexe 3 – Lac Bélanger : Résultats des pertes au feu. Contenu en eau (gauche); Contenue en matière organique (centre); Contenu en carbonates (droite).

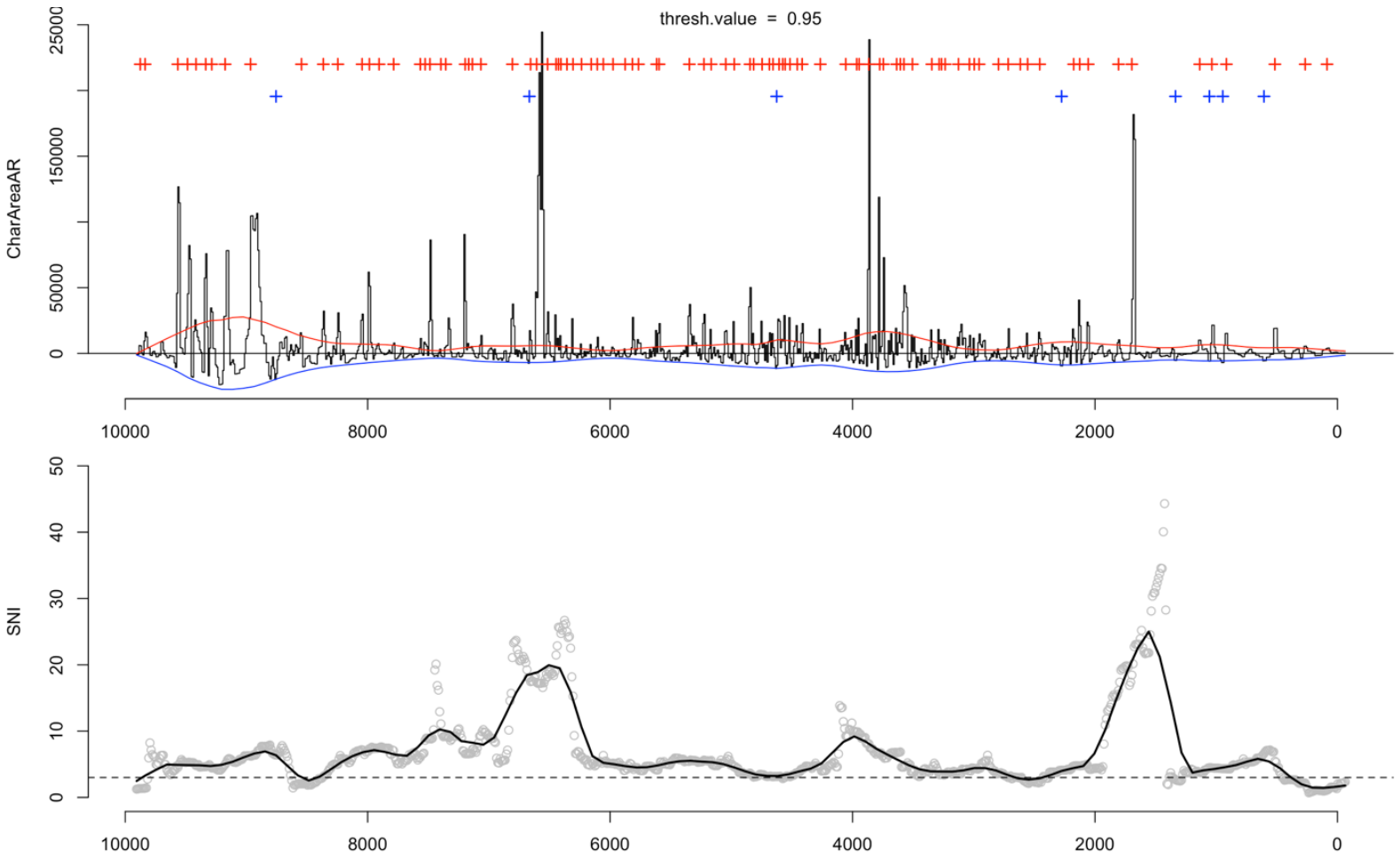

Annexe 4 – Lac Bélanger : Accumulation de charbons (μm^{-2} . cm^{-2} . an^{-1}) en fonction du temps (années cal. BP.). Les pics positifs sont identifiés par des croix rouges et les pics négatifs par des croix bleues (haut); SNI (*Signal to Noise Index*; courbe noire) en fonction des événements de feux (points gris) et du temps (années cal. BP.) (bas). Obtenu à l'aide de la librairie R *tapas (Finsinger et Bonnici, 2022)*

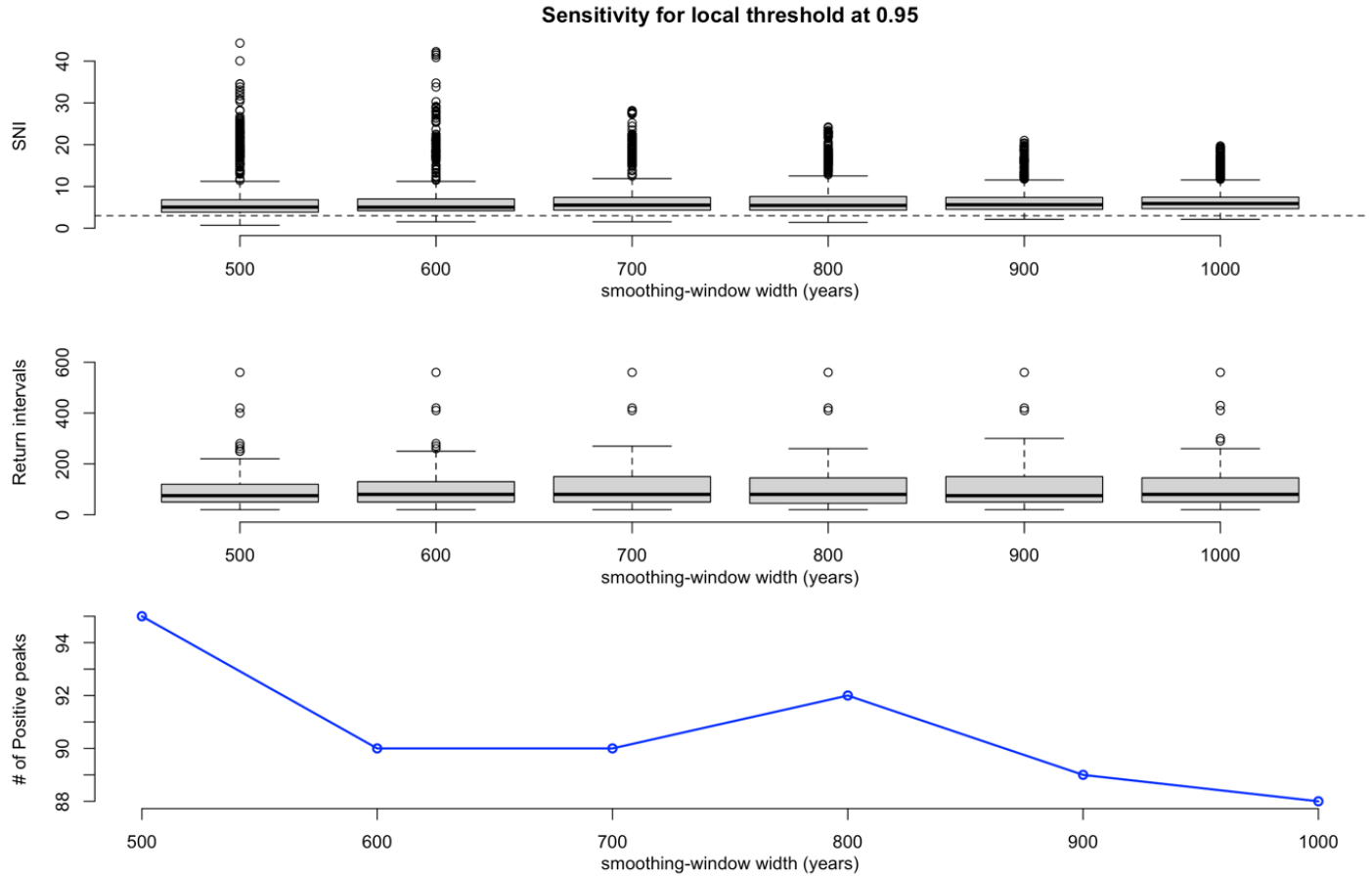

Annexe 5 – Lac Bélanger : Distribution du SNI en fonction de la fenêtre temporelle choisie (Haut); Intervalle de retour des feux en fonction de la fenêtre choisie (Milieu); Nombre de pics de charbons en fonction de la fenêtre choisie (bas). Obtenu à l'aide de la librairie R *tapas (Finsinger et Bonnici, 2022).*